



THESIS APPROVAL

GRADUATE SCHOOL, KASETSART UNIVERSITY

Doctor of Engineering (Chemical Engineering)

DEGREE

Chemical Engineering

FIELD

Chemical Engineering

DEPARTMENT

TITLE: Development of Au/CeO₂/Al₂O₃ Catalytic Membrane Reactor Via
Electro-spinning and Sol-Gel Techniques for Water Gas Shift Reaction

NAME: Miss Kanchana Luepong

THIS THESIS HAS BEEN ACCEPTED BY

THESIS ADVISOR

(Associate Professor Paisan Kongkachuichay, Ph.D.)

THESIS CO-ADVISOR

(Mr. Piyawit Koombhongse, Ph.D.)

DEPARTMENT HEAD

(Associate Professor Phungphai Phanawadee, D.Sc.)

APPROVED BY THE GRADUATE SCHOOL ON _____

DEAN

(Associate Professor Gunjana Theeragool, D.Agr.)

THESIS

DEVELOPMENT OF Au/CeO₂/Al₂O₃ CATALYTIC MEMBRANE REACTOR VIA ELECTRO-SPINNING AND SOL-GEL TECHNIQUES FOR WATER GAS SHIFT REACTION

KANCHANA LUEPONG

A Thesis Submitted in Partial Fulfillment of
the Requirements for the Degree of
Doctor of Engineering (Chemical Engineering)
Graduate School, Kasetsart University

2010

Kanchana Luepong 2010: Development of Au/CeO₂/Al₂O₃ Catalytic Membrane Reactor Via Electro-spinning and Sol-Gel Techniques for Water Gas Shift Reaction. Doctor of Engineering (Chemical Engineering), Major Field: Chemical Engineering, Department of Chemical Engineering. Thesis Advisor: Associate Professor Paisan Kongkachuichay, Ph.D. 78 pages.

This research was focused on developing a catalytic membrane reactor (CMR) assembling of three layers: supporting layer, gas separating layer, and catalytic layer that were made of porous alumina disk, alumina gel synthesized via a sol-gel technique, and ceria (CeO₂) fibers doped with gold synthesized via electrospinning technique, respectively. The fabricated CMR was used for converting CO to CO₂ and H₂ through the water gas shift reaction. The alumina layer was prepared by hydrolyzing aluminum tri-sec butoxide mixed with i-butanol as diluent. The acetylacetone (ACAC) was added into the mixed solution to control the gel morphology. The gel was aged at room temperature for 2 days then it was calcined at 500°C for 1 hour. The obtained alumina was found to have 36 Å pore size diameter with narrow distribution, 560.3 m²/g surface area, and 0.6 cc/g pore volume. Subsequently, it was spin-coated on the porous alumina disk forming the gas separating layer having 1 mm thickness. Before fabricating the ceria layer via electrospinning process, the effect of co-solvent (i-propanol and water), supplied electrical voltage, and distance between needle tip and ground collector were studied to determine the optimum condition for spinning ceria fibers. Consequently, the smooth electrospun fibers were produced using 50 wt % of i-propanol, 18 kV electric field, and 8 cm distance between needle tip and collector. After calcined at 450°C for 3 hours, the obtained fibers were confirmed to be ceria structure having an average diameter of 600 ± 80 nm. Then the ceria fibers were spun and deposited on the alumina gel layer and incipient wetness impregnated with HAuCl₄.

Finally, the water gas shift reaction was conducted in three types of reactors composing of the same catalyst (Au/CeO₂/Al₂O₃): fixed bed, CMR, and hybrid CMR (fixed bed combined with CMR). At the optimum condition, 250°C and 45 min, the corresponding CO conversion was, 52.31, 21.78 and 97.69, respectively. Therefore, the hybrid CMR yielded the best performance.

Student's signature

Thesis Advisor's signature

ACKNOWLEDGEMENTS

I wish to special acknowledge to Assoc. Prof. Dr. Paisan Kongkachuichay, my thesis advisor, for his great guidance over the course of my graduate career. I would like to thank my co-advisor, Dr. Piyawit Koombhongse, and all of thesis committees for their suggestions and valuable times to fulfill my research.

I thankfully acknowledge the financial support from Rajamangala University of Technology Phra Nakhon. This work was supported in part by Kasetsart University Research and Development Institute (KURDI) and the National Center of Excellence for Petroleum, Petrochemicals, and Advanced Materials (PPAM). I would also thank Mr. Payoon Santhongkaew, Department of Material Engineering who designed, created, repaired my reactor, and his encouragement. Also, I would like to thank the PSK's Lab members at the Chemical Engineering Department, Kasetsart University.

Finally, my appreciation devotes to my family who always give me heartfelt supports.

Kanchana Luepong
March 2010

TABLE OF CONTENTS

	Page
TABLE OF CONTENTS	i
LIST OF TABLES	ii
LIST OF FIGURES	iii
INTRODUCTION	1
OBJECTIVES	6
LITERATURE REVIEW	8
MATERIALS AND METHODS	24
Materials	24
Methods	25
RESULTS AND DISCUSSION	35
CONCLUSION AND RECOMMENDATIONS	59
Conclusion	59
Recommendations	61
LITERATURE CITED	63
APPENDICES	69
Appendix A Gas calibration curves	70
Appendix B Water gas shift reaction process	75
CURRICULUM VITAE	78

LIST OF TABLES

Table		Page
1	The effect of i-propanol on solution viscosity	35
2	The fiber morphology at the different electric field	37
3	The morphology fiber at the different distance	38
4	Elemental composition on the fibers	42
5	N ₂ -adsorption analysis of calcined alumina synthesized by using different molar ratio of water/alkoxide	44
6	N ₂ -adsorption analysis of calcined alumina synthesized by using different molar ratio of ACAC	46
7	N ₂ -adsorption analysis at the different sintering temperature	47
8	N ₂ -adsorption analysis at the different sintering time	49
9	Gas adsorption (%) through the ceramic membrane layer	51
 Appendix Table		
A1	CO calibration curve	71
A2	CO ₂ calibration curve	72
A3	H ₂ calibration curve	73
B1	The reactor comparative on the water gas shift reaction	76
B2	The water gas shift condition	77

LIST OF FIGURES

Figure		Page
1	Schematic diagram of fuel processing system	2
2	Schematic of carbon monoxide reduction	2
3	Principle of membrane reactors	11
4	The membrane coupling with catalysts	12
5	Schematic diagram of the electrospinning process	14
6	Sol-gel process	21
7	Flow diagram of this work	25
8	Electrospinning equipment set up	27
9	Gas interaction performance set up	29
10	Catalytic membrane composition	32
11	Reactor types in this study	33
12	Schematic diagram of water gas shift reaction	34
13	Electrospun fiber obtained at 6 kV (a) and 18 kV (b)	37
14	Merged fiber obtained at 6 cm	39
15	SEM micrograph at 18 kV and 8 cm distance	39
16	Thermal behavior of the mixed solution	40
17	SEM micrographs of fibers before (a) and after (b) calcination	42
18	XRD pattern of synthesized fibers	43
19	Size distribution by the different water concentration	45
20	Size distribution of synthesized alumina by ACAC varying	46
21	Size distribution by the different temperature sintering	48
22	Size distribution by the different time sintering	49
23	SEM photographs of synthesized alumina (a) and its size distribution (b)	50
24	SEM photograph of alumina supported disk	52
25	SEM photograph of synthesized alumina	53

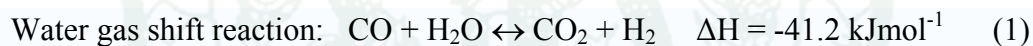
LIST OF FIGURES (Continued)

Figure	Page
26 SEM photographs of cross section (a) and topped view (b) of catalytic membrane layer	53
27 CO conversion (X_{CO}) by the different reactor type	55
28 CO conversion (X_{CO}) on fixed bed reactor	56
29 CO conversion (X_{CO}) on catalytic membrane reactor	56
30 CO conversion (X_{CO}) on hybrid membrane reactor	57
31 CO conversion (X_{CO}) at 250°C for 45 min	58
 Appendix Figure	
A1 CO Calibration curve	72
A2 CO ₂ Calibration curve	73
A3 H ₂ Calibration curve	74

DEVELOPMENT OF Au/CeO₂/Al₂O₃ CATALYTIC MEMBRANE REACTOR VIA ELECTRO-SPINNING AND SOL-GEL TECHNIQUES FOR WATER GAS SHIFT REACTION

INTRODUCTION

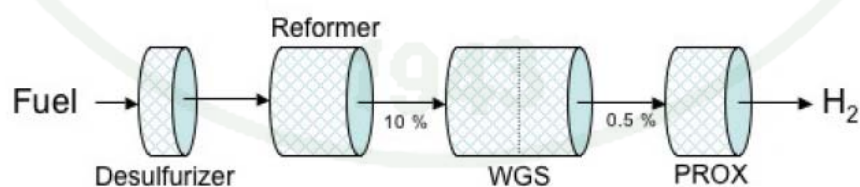
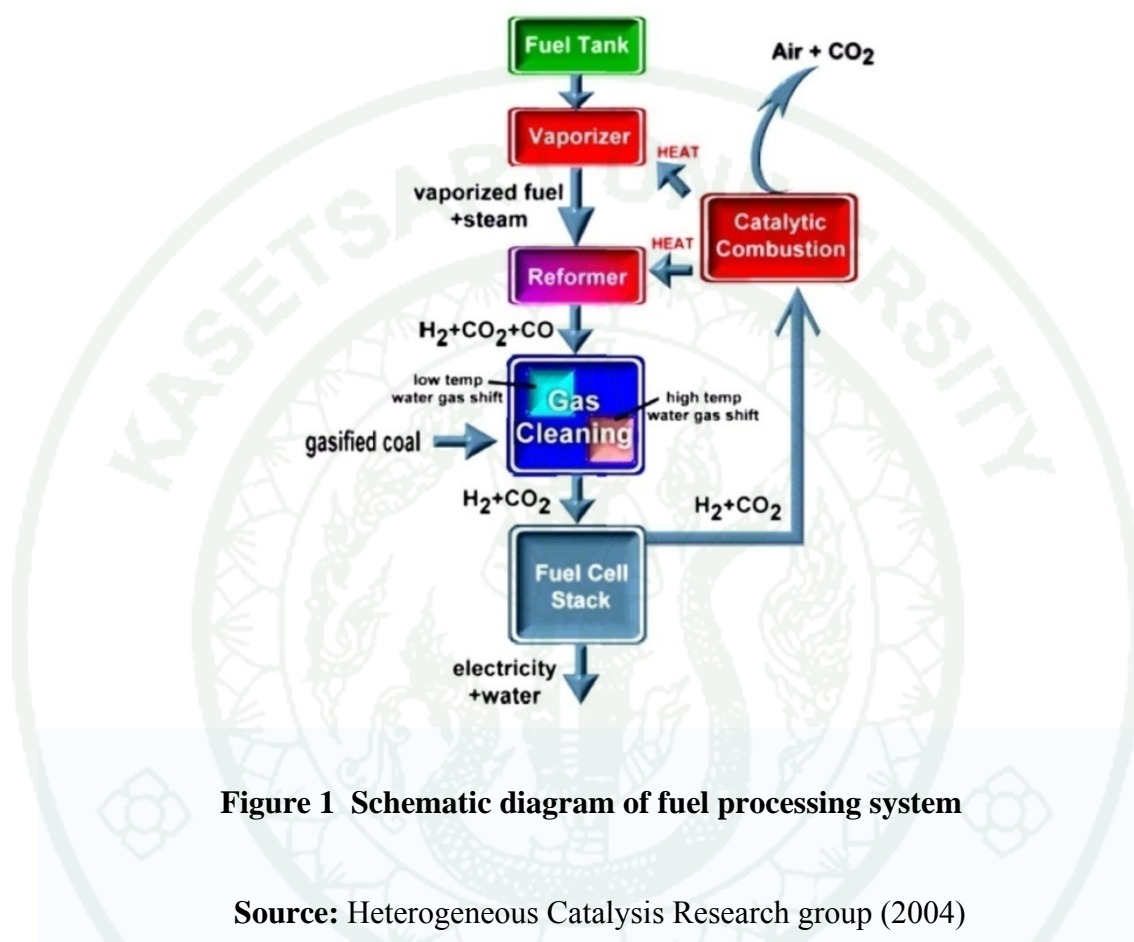
The water gas shift reaction is an inorganic reaction in which carbon monoxide (CO) reacts with water vapor (H₂O) to form carbon dioxide (CO₂) and hydrogen (H₂) as shown in equation 1. It is an important role in manufacturing hydrogen process, ammonia, methanol and other chemicals industrial. It is used in conjunction with steam reforming of methane or other hydrocarbons, which is important for the hydrogen high purity production. In fuel-rich hydrocarbon combustion processes, the water gas reaction at equilibrium state is employed as a means to provide estimates for molar concentrations of burnt gas constituents.



This reaction is exothermic and H₂ product is thermodynamically favored at low temperature (e.g. 175 – 250°C) and high steam ratios. The water gas shift reaction is sensitive to temperature, with the tendency to shift towards reactants as temperature increases due to Le Chatelier's principle.

In addition, the water gas shift reaction is a renewed interesting reaction in proton exchange membrane fuel cell power (PEMFC). It can remove a poisoning gas as CO from the system. The schematic diagram is shown in Figure 1. Hydrogen is widely seen as a clean energy carrier for future use in both transportation and electricity sectors. The syngas requires further processing through the water gas shift reaction in order to maximize H₂ production. This reaction has been commercially used and developed over many decades.

The fuel processing system requires hydrogen with a low CO concentration, hence water gas shift reaction is capable to reduce the CO contaminants from 10 to 0.5 mole % wet basis. The carbon monoxide reduction is shown in Figure 2.



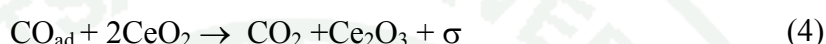
Due to thermodynamic equilibrium limitations, the typical water gas shift reaction is divided into two temperature regimes. The one is a high temperature shift reaction at 310 to 450 °C, the high-temperature shift commercial catalysts are Fe_2O_3 and Cr_2O_3 . Another one is a low temperature shift reaction at 195 to 250°C using Cu-ZnO, and Al_2O_3 as commercial catalysts. However, these catalysts are unsatisfied using in fuel processing due to their complex and time-consuming activation protocol before use and instability when contact with air. Consequently, it is a critical point to develop new water gas shift catalysts with high activity and stability over a wider operating temperature window that is currently possible with the commercial shift catalysts. The alternative catalysts containing the noble metal e.g. Pt, Rh, Ru, Pd, and Au supported on oxide and mixed oxide substrates have been proved to be very effective having superior performances for the water gas shift reaction.

It is generally accepted that the water gas shift reaction occurs in a bifunctional manner with the participation of both the noble metal and the support. One of the proposed mechanism is the redox process, whereby CO adsorbed onto the metal is oxidized by the support (Gonzalez *et al.*, 2008). The other mechanism uses to describe the water gas shift reaction is the associative mechanism, in which formate production on the surface by CO reaction with OH groups of supports participates as intermediates decomposing to hydrogen and unidentate carbonate prior to the liberation of CO_2 .

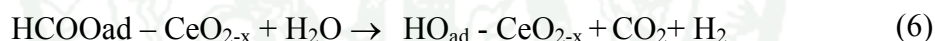
Recently, it has been reported that gold (Au) supported catalysts are interesting candidates for novel water gas shift reaction (Li *et al.*, 2008). It is generally known that high catalytic activity of the gold/metal oxide catalysts depend strongly on the dispersion of gold particles and their interaction between gold and support. Au has been studied frequently as a catalyst or co-catalyst.

The water gas shift catalyst based on ceria (CeO_2) has been investigated as alternative to Cu-ZnO catalyst for fuel processing. Ceria is well-known as an oxygen storage material. Especially, Au/ CeO_2 catalyst has shown to be very active catalyst for the low temperature water gas shift reaction because it has high activity at even

lower temperature. There are two major reaction mechanisms have been proposed for the water gas shift reaction over ceria-based catalysts: redox and formate mechanism. Based on the oxygen storage ability of ceria-supported catalysts, the redox reaction will occur on precious metals supported by ceria. The redox mechanism is shown in the following steps: (Bunluesin *et al.*, 1998 and Chen *et al.*, 2008)



Where σ represents a free adsorption site on the metal surface and CO_{ad} is the adsorbed CO on the metal surface. Metal adsorbed CO can be oxidized by CeO_2 to form CO_2 and Ce_2O_3 . Then, water oxidizes Ce_2O_3 to yield CeO_2 and H_2 . The formate mechanism is shown in the following steps: (Chen *et al.*, 2008)



For water gas shift reaction, under wet condition the formate mechanism is a dominating step. Therefore, the mechanism in catalysis process of gold containing system generally forms carbonyl or carbonate-like species on ultrafine gold particle (Li *et al.*, 2008). These species will block the active sites that contribute to deactivate of Au/ CeO_2 catalyst. In order to avoid this problem, solid sorbent such as zeolite, activated carbon, and alumina is employed as selective chemisorption (Michael *et al.*, 2009).

Electrospinning is a basic process that a high voltage extrudes a viscous polymer jet solution through a capillary to a collector. This technique is similar to traditional technique e.g. melt spinning or solution spinning, except electrostatic repulsions are utilized to stretch a viscoelastic fluid instead of pressure driven flow through an extruder. Electrospinning has generated significant attention since this technique forms fibers on the order of 1 μm down to 100 nm in diameter, 2 to 3

orders of magnitude smaller than conventionally spun fibers. The products are continuous and randomly packed over a supporter. They achieve a high specific surface area to volume ratio, high porosity, and continuous fibers. Due to their advantages, the unique fibers have been suggested for many applications, for example drug delivery, filtration process, membranes, vascular grafts, protective clothing, optical sensors, and tissue scaffolds. The fiber morphology and diameter depend on the effects of processing variables including applied voltage, tip to target distance, feed rate of the solution, and the solution properties (e.g. type of solvent, viscosity, concentration, conductivity, surface tension).

A catalytic membrane reactor (CMR) is a new reaction scheme that combines a chemical reaction with a separation process. It is a plug flow reactor that contains an additional porous cylinder inside another shell. This porous inner cylinder is the membrane that gives the membrane reactor its name. A catalytic membrane reactor has a coated membrane or makes of a catalytic containing materials, which means that the membrane itself participates in the reaction. Some of the reaction products that are small enough can pass through the membrane and exit the reactor on the permeate side.

In this work, a catalytic membrane reactor was used to convert CO to CO₂ via the catalytic membrane and the gas separation layer were fabricated by electro-spinning and sol-gel techniques. This novel designed reactor was expected to yield the better performance than the conventional fixed-bed reactor.

OBJECTIVES

The objective of the present work is to fabricate a catalytic membrane reactor via electrospinning process and sol-gel technique. The main objective can be broken down into the following:

1. To synthesize and characterize the catalytic membrane reactor (CMR) via electrospinning process and sol-gel technique
2. To study the catalytic performance of the obtained CMR on the water gas shift reaction compared with a fixed bed reactor

Scope of work

In order to achieve the objectives, there were two investigated parts. These were synthesis and performance parts. The details are described as follows:

1. Part I: Catalytic Membrane Synthesis

1.1 Catalytic membrane layer

Catalytic membrane was cerium oxide (CeO_2) fiber synthesized via electrospinning process impregnated with gold colloid (HAuCl_4). It was prepared by using the co-solvent between i-propanol and water. The studied parameters were solution viscosity, electric field, and distance between tip and collector.

1.2 Ceramic membrane layer

Ceramic membrane was made of alumina (Al_2O_3) that was synthesized by sol-gel method using aluminum tri-sec butoxide as precursor. The considered parameters were water content, acetylacetone (ACAC) content, sintering temperature and sintering time.

2. Part II: Water gas shift reaction performance

The water gas shift reaction was carried out in three reactor types: a fixed bed reactor, a catalytic membrane reactor, and a hybrid membrane reactor. The examined conditions were 225, 250, and 275°C for 15, 45, and 75 minutes, respectively.



LITERATURE REVIEW

Water gas shift reaction

The water gas shift reaction is an old industrial process in which water as steam is mixed with carbon monoxide to obtain hydrogen and carbon dioxide. It has found new significance in fuel processing, in conjunction with fuel cells. The water gas shift reaction is reversible and exothermic ($\Delta H = -41.2$ kJ/mol). Due to its moderate exothermic reaction, the water gas shift reaction is thermodynamically unfavorable at elevated temperatures. The kinetics reaction of the catalytic is more favorable at higher temperatures. In order to overcome this thermodynamic limitation while maintaining high reaction rates, it is normally conducted in multiple adiabatic stages with inter-stage cooling to obtain higher conversions overall. The high temperature shift (HTS) is conducted in the first stage where operation temperatures range 310°C to 450°C, while low temperature shift (LTS) occurs in the second stage with a temperature range of 195°C to 250°C. Different catalysts are employed in the two different stages.

For HTS operation, the catalyst is typically a combination of Fe_3O_4 , the stable iron phase under reaction conditions, and chromium that help minimizing sintering effect by textural promotion. The HTS reactor must maintain an inlet temperature of 350°C in order to achieve an adequate reaction rate. The maximum temperature is limited to 530-550°C. The temperature rises due to the exothermic nature of the water gas shift reaction. The operating pressure is determined by the other steps in the process, but may be as high as 3 MPa. The current typical LTS catalyst is a substantially improved version of the copper liquor used to remove CO from processes prior to 1962. The commercial LTS catalyst is composed of copper, zinc oxide, and alumina. The copper and zinc oxide forms are stable under reactions conditions. Copper, the active specie, remains active at temperature as low as 200°C. The zinc oxide provides some protection of the copper from sulfur poisoning by reaction with adsorbed sulfur compounds while acting partially as a support for the copper. The commercial LTS catalyst is more sensitive to deactivation caused by sintering than the HTS catalyst. This causes the maximum operating temperature to

be only around 250°C, typically. When used in conjunction with HTS, the exit gas stream from the HTS unit must, therefore, be cooled, usually by quenching with water providing additional steam to the process, before passing through the LTS unit.

The water gas shift reaction is not only important for generating hydrogen, it is also useful to decrease the CO concentration in hydrogen-rich effluent from reforming units (Aquila *et al.*, 2008). An emerging application for the water gas shift is in the production of hydrogen for proton exchange membrane fuel cells. This reaction is important because it removes CO, a poison to the electrocatalysts, which is produced during the steam reforming and/or partial oxidation reactions (Li *et al.*, 2008). The latter is of particular importance for potential applications such as polymer electrolyte fuel cells. Therefore, CO concentration must be reduced to about 10-50 ppm to avoid efficiency losses (El-Moemem *et al.*, 2008).

The reaction assisted by a catalyst membrane reactor was previously studied in a few works. All of them carried at the high temperature regime. Seok and Hwang (1990) used ruthenium (III) chloride trihydrate on porous Vycor glass to evaluate the performance of the water gas shift reaction using a catalyst membrane reactor. They found that 85 % conversion of CO at 430 K (157°C) with the permeate rate 0.64 cm³/min was obtained. However, this conversion was still lower than the equilibrium conversion. Later, Kikuchi and Uemiya (1991) developed a double tubular type membrane reactor using iron chromium oxide as catalyst coated on thin palladium film (inner tube). They achieved complete conversion of CO at 673 K (400°C). In addition, it was found that the level of CO conversion was depended on the thickness of the palladium film. However, Basile *et al.* (1996) compared reaction by using ultrathin palladium tubular reactor prepared by co-condensation technique. The reaction temperature was 600 K (327°C) and CO conversion 99.89% was achieved. They claimed that the CO conversion depended on the sweep gas flow (N₂). That was corresponding to Karnik *et al.* (2001) fabricated the palladium based micromembrane for water gas shift reaction and hydrogen gas separation. The membrane composed of 4 layers: copper, aluminum, spin-on-glass (SOG), and palladium. Copper, aluminum and SOG layers were perforated. The palladium film served as a structural support

for the main element of the membrane. Copper acted as the catalyst in the water gas shift reaction. At 250°C copper catalyzed the conversion of carbon monoxide to hydrogen gas that was subsequently separated selectively through the palladium membrane thus shifting the reaction to product side. The membrane strength was very important because the hydrogen gas passed through the membrane was driven by a pressure gradient across it.

In the recent years, the precious metals are the alternate catalysts in low temperature water gas shift reaction. They offer greater CO conversion but are still expensive. Therefore, the most researchers try to use them altogether with cheaper materials as co-catalysts e.g. Pt/SnO₂, Pt/C, Cu-Pd/CeO₂, Pt/CeO₂/Al₂O₃, (Cu, Ag, Au)/CeO₂. The Ag/ceria was found to be inactive for the reaction because it adsorbed very few CO. A supported on ceria has been reported as effective catalyst for CO oxidation, and the low temperature water gas shift reaction (Yuan *et al.*, 2007 and El-Moemem *et al.*, 2008). However, other noble metal deposited over cerium was observed such as platinum (Gonzalez *et al.*, 2008), Ni-Mn-K/bauxite (Lilong *et al.*, 2008), and Vanadium-promoted Pt/CeO₂ (Andera *et al.*, 2008). All of them purpose and challenges due to application in generation systems based on fuels cells. A relationship between the water gas shift activity of metal-supported catalysts and the heat of CO adsorption (Callaghan, 2006) i.e., metals that chemisorb CO weakly, such as Au, have a low activity due to the low concentration of surface CO. The optimum strength of CO chemisorptions on metals was identified as 20 kcalmol⁻¹. The Au-CO bond strength is found to be in this energy range.

Catalytic membrane reactor

Nowadays, membrane technologies are more frequently used for separation of wide varying mixture industrials and can complete successfully with traditional schemes. There are attractive in petrochemical industry, gas separation application, and environmental by wastewater usage as bio reactor process. A membrane reactor is a device that combines a membrane separation or distribution process with a chemical reactor in one unit (Li, 2007). Due to the integration of reaction and

separation or distribution in chemical processes become simpler leading to a much lower processing cost. In addition, membrane reactors are capable of promoting a reaction process by: 1) selectively removing at least one of the products from the reaction zone through the membrane, making the equilibrium reaction shifting to the product side; 2) supplying only a particular reactant to the reaction zone giving an optimum concentration ratio of the two reactant streams. As a result, the yield can be increased even though beyond the equilibrium value for equilibrium reactions and/or the selectivity can be improved by suppressing other undesired side reactions or the secondary reaction of products. The membrane principles illustrated in Figure 3.

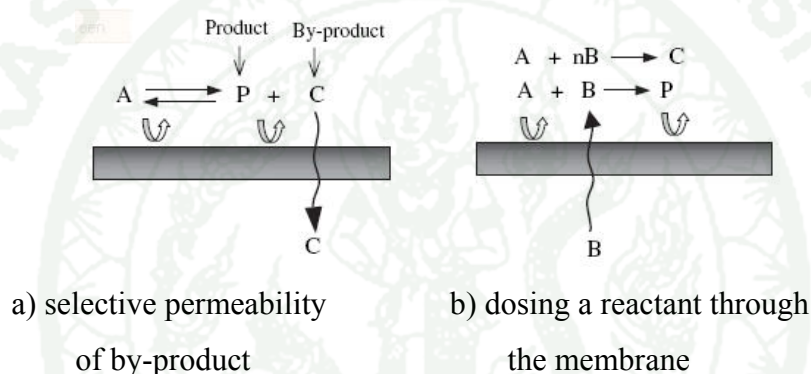


Figure 3 Principle of membrane reactor

Source: Li (2007)

Membrane gas separation is an attractive utilization. It is a simple process having low energy cost. However, it has one major drawback that is a reverse relationship between selectivity and permeability. There is high potential energy saving behind membrane gas separation because the separation process takes place without phase transition. The development of novel materials for gas membrane manufacturing such as organic polymer, hybrid organic-inorganic materials are expanding the use of membrane technology. Nanocomposite membranes can improve the selectivity and gas permeability simultaneously. Membrane is defined as a barrier that separates two phases and restricts transport of various chemical in a selective manner. The process of gas permeation is a relatively simple process which

has been expanded commercially since 1979. The application covers the supply of pure or enriched gases such as He, N₂, and O₂ from air, acid gases such as CO₂ and H₂S, and H₂ separation in the petrochemical and chemical industries.

The catalytic membrane reactors are coupling of the membrane with catalysts. It is configured basically in three ways (Li *et al.*, 1996). The membrane coupling is illustrated in Figure 4.

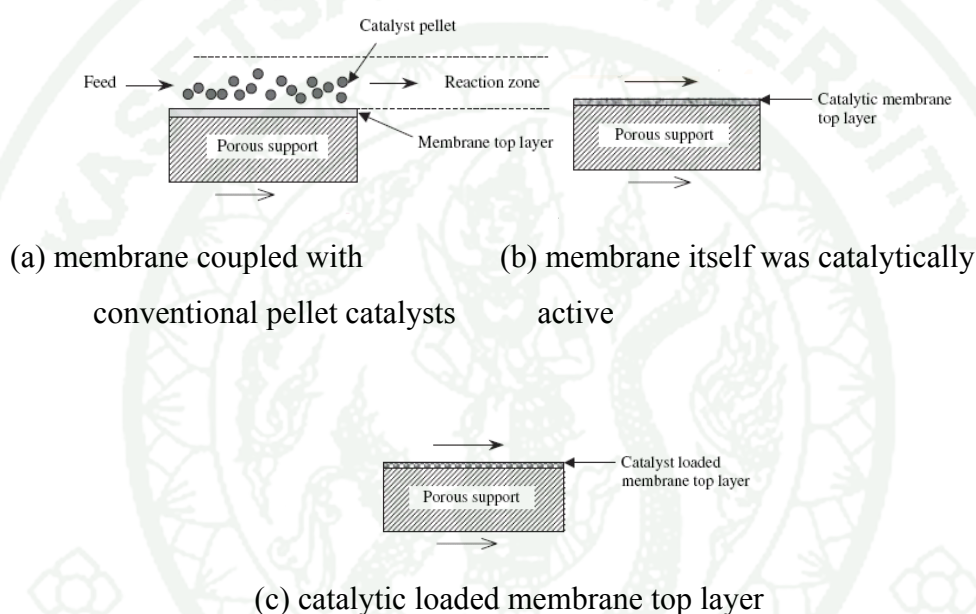


Figure 4 The membrane coupling with catalysts

Source: Li (2007)

In Figure 4 (a) the membrane is coupled with conventional catalysts pellet. It should be noted that the membrane layer, which facilitates the separation is forms only a small part of the overall membrane thickness, with the support layer forming the major part. This configuration has been mostly applied in dehydrogenation reactions. Sometimes, the catalyst in the form of paste is coated on the membrane top layer, but it functions in a similar way to the pellet catalyst. In the second arrangement, the membrane itself is catalytically active as shown in Figure 4 (b). The active catalyst is a thin dense membrane layer deposited on a surface of a porous

support. A potential problem with this configuration is that the membrane may not have sufficient catalytic area to be totally effective. The final configuration shown in Figure 4 (c) is for a catalyst impregnated into the pores of a microporous material either as individual particles or as a layer. This is a convenient way of introducing catalyst into the membrane and has also been used in dehydrogenation reactions.

The catalytic membrane application is a long history. The first application was used as flow-through reactor (Yamada *et al.*, 1988) by means of anodic oxidation of aluminum plates and subsequent removal of the membrane from the substrate. The catalytic membrane was prepared with a 5-50 μm thickness for single-sided oxidation and 50-100 μm for double-sided oxidation, respectively. The reaction was set up from one side to the other through the catalytic membrane to indicate fluid permeates. The anodized alumina film was a similar catalytic activity with isomerization of 1-butene membrane reactor. The potential applications were in flue gas cleaning (Saracco and Specchia, 1995). The catalytically active ceramic porous filtered mechanically particles by applying $\gamma\text{-Al}_2\text{O}_3$ layer. The catalytic membrane decomposed the chemical pollutants as NO_x and Volatile organic compound (VOC) by flow through forcing. The wider pores were an obvious alternative. It applied mixed-regime catalytic membrane to the VOC combustion (Pina *et al.*, 1996 and Zalamea *et al.*, 1999). The identification was considered on Knudsen-diffusion diffusion system with a homogeneous tubular structure of $\gamma\text{-Al}_2\text{O}_3$. The Pt catalyst was deposited on tubular by wet impregnation. The partial oxidation of alkane was an aspect for catalytic membrane reactor (Frusteri *et al.*, 2000). The reaction was affected H_2O_2 in the presence of Fe^{2+} catalyst under mild condition. A reaction pathway by involved the electrophilic activation of paraffin on superacid sites and the subsequent reaction with OH radicals generating according Fenton chemistry. The other integration of the micro membrane reactor was designed to process of gas mixture in gas analyzing system (Splinter *et al.*, 2002). The CO selectivity was increased by allowing CO_2 passing through the catalytic membrane. The gas-phase oxidation of methanol was a model volatile organic component in a photocatalytic membrane reactor (Tsuru *et al.*, 2003). The several nanometers TiO_2 catalyst membrane was deposited on cylindrical α -alumina microfiltration membrane. The

methanol decomposition rate was investigated in an air stream. The higher decomposition rate contributed. The force convection transported enhanced at the larger surface area.

Electrospinning process

Electrospinning process is not a new technology for polymer fiber production. It has been known since the 1930's to produce nanofibers. An experimental setup was outlined for the production of polymer filaments using electrostatic force. When used to spin fibers this way, the process is termed as electrospinning. In other words, electrospinning is a process that creates nanofibers through an electrically charged jet of polymer solution or polymer melt. The electrospinning process, in its simplest form consisted of a pipette to hold the polymer solution, two electrodes and a DC voltage supply in the kilovolt range. The schematic diagram presented in Figure 5.

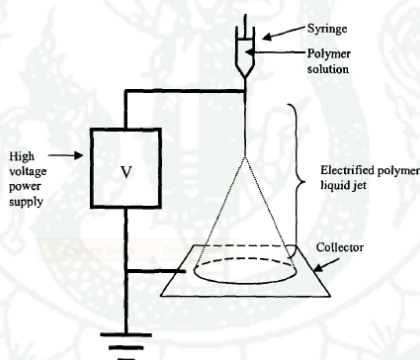


Figure 5 Schematic diagram of the electrospinning process

Source: Ramakrishna *et al.* (2005)

In Figure 5, the polymer drop from the tip of the pipette was drawn into a fiber due to the high voltage. The jet was electrically charged and the charge caused the fibers to bend in such a way that every time the polymer fiber looped, its diameter was reduced. The fiber was collected as a web of fibers on the surface of a grounded target.

Important features of electrospinning are (Ramakrishna *et al.*, 2005):

1. Suitable solvent should be available for dissolving the polymer.
2. The vapor pressure of the solvent should be suitable so that it evaporates quickly enough for the fiber to maintain its integrity when it reaches the target but not too quickly to allow the fiber to harden before it reaches the nanometer range.
3. The viscosity and surface tension of the solvent must neither be too large to prevent the jet from forming nor be too small to allow the polymer solution to drain freely from the pipette. The power supply should be adequate to overcome the viscosity and surface tension of the polymer solution to form and sustain the jet from the pipette.
4. The gap between the pipette and grounded surface should not be too small to create sparks between the electrodes but should be large enough for the solvent to evaporate in time for the fibers to form.

Since electrospinning is basically the drawing of a polymer fluid, there are many different types of polymers and precursors that can be electrospun to form fibers. The materials to be electrospun will depend on the applications. Materials such as polymers and polymer nanofiber composites can be directly produced by electrospinning. Other materials such as ceramics and carbon nanotubes require post processing of the electrospun fibers.

The materials and application of electrospun fibers are numerous, individual material properties must be considered depending on its applications. The electrospinning process may be modified so as to yield electrospun fiber with the desired morphology and properties. When used as composite, the nanofibers can be made as a composite on its own or it can be used as reinforcement in a matrix. In the production of ceramic fibers, post processes are required after the fibers are electrospun. Thus it is important to have a basic understanding of the different group

of materials before selecting the most appropriate electrospun fibers for specific applications.

Many kind of polymer have been used to produce polymeric nanofibers. They can be achieved from optimum viscosity polymer were feeding out to the ground collector. The obtained nanofibers have diameter ranging around 40 - 200 nm and fluffy structures. They yield more powerful application than that of the conventional process when some compounds or some metals were added. The polymer fibers were produced in any application. A terpolymer synthesized consisted of a backbone with two kinds of functional side chains: one with quaternary structure and the other with perfluorinated structure for hydrophobic nature (Acatay *et al.*, 2003). The obtained electrospinning fibres exhibited antibacterial activity (Grafe *et al.*, 2003). It was fabricated nanofiber webs from any polymer to increase the filtration efficiency. Also, the silver (Ag) nanoparticles (Yang *et al.*, 2003) were filled into polyacrylonitrile (PAN) nanofibers to enhance the conductivity than the pure polymer solution.

Till date, there are many polymers that have been electrospun including custom made polymers. The non-biodegradable synthetic polymers with the corresponding solvent and concentration are widely used to yield fibers without beads. Electrospun fibers are commonly used in the field of tissue engineering due to their small diameters which are able to mimic natural extracellular matrix. Thus there are two groups of polymers that are commonly electrospun: biodegradable polymers and natural polymers.

Unlike polymer, where there is usually no need for post-electrospinning process, ceramics nanofibers can be made from electrospinning of the ceramic precursors and followed by sintering of the electrospun fibers to derive ceramic fibers such as titanium dioxide nanofibers from inorganic precursor and polymer content (Ding *et al.*, 2004), ZrO₂ nanofibers (Shao *et al.*, 2004), and nickel titanate/polyvinyl acetate composite nanofibers (Dharmaraj *et al.*, 2004). This process involved the preparation of sol solution to achieve the right rheology for

spinning process. Spinning of the obtained solution yielded polymer/inorganic composite nanofibers then they were calcined to attain final oxide nanofibers.

Whilst it is a membrane macroscopically, the membrane is a network of nanofibrous structure. Hence the terms nanofiber membrane, nanofiber mesh and nanofiber web are used interchangeably in order to reflect the diversity of viewpoints. These terms, as well as other technical terms, are defined and explained in the benefit glossary. Therefore, electrospinning process had a great benefit to produce the nanofibers in secondary application as filtration, electricity application and membrane application. It is an interested choice to produce the catalytic membrane for water gas shift reaction.

Ceria (CeO₂)

Ceria (CeO₂) is an interesting metal oxide which has unique properties. It is able to shift between reduced and oxidized states ($\text{Ce}^{3+} \leftrightarrow \text{Ce}^{4+}$) easily and accommodate variable levels of bulk and surface oxygen vacancies. These abilities make it suitable to be used as a support as well as catalyst in processes wherein reaction conditions fluctuate between oxidation and reduction. CeO₂ plays multiple roles in various catalyst systems and it is understood that CeO₂ promotes noble metal dispersion, increases thermal stability of Al₂O₃ support (Reddy *et al.*, 2005), promotes water gas shift and steam reforming reaction, favors catalytic activity at the interfacial metal-support sites, and promotes CO removal through oxidation by employing its lattice oxygen, stores and releases oxygen under lean oxygen and rich conditions. Therefore, CeO₂ have been receiving a great attention deal in recent years due to their widespread using in many applications e.g. catalysis to ceramics, fuel cell technologies, gas sensors, solid state electrolytes, chromatographic materials, cosmetic, etc. Hence, the CeO₂-containing materials are very express growing in technological applicability. Despite CeO₂ widespread applications thus the pure ceria is highly discouraged since it is poorly thermo stable as it undergoes sintering at high temperature. The high temperature causes the loss of crucial oxygen storage and release oxygen during operating condition, other transition and non-transition metal

ions could be introduced into the ceria cubic structure. Of course, the redox and catalytic properties of CeO_2 are strongly influenced when it is combined with other transition metals.

CeO_2 -containing materials application was reported in many works e.g. Fe-doped CeO_2 by ordinary methods and terahertz-time domain spectrometer (THz-TDS) technique (Wen *et al.*, 2009). They found pure CeO_2 only has a small dielectric constant of 4 but the power absorption and the index of refraction increase with frequency, while Fe was doping into CeO_2 . They were potentially in THz optical material. The other, the $\text{Si/CeO}_2/\text{SiO}_2$ was an effect on crystal phase of silicon structure (Milovzorov, 2008). And the Pt/Ce on the metal support for the water gas shift reaction was present in a few published. The Pt/Ce- TiO_2 (Gonzalez *et al.*, 2008) was enhanced performance in the water gas shift reaction by Pt deposited over a cerium-modified TiO_2 . The Pt/Ce- TiO_2 facilitated the reducibility of the support at low temperature while Ce-O-Ti surface interactions established in the Ce-modified support TiO_2 . Ce-modified decreased the over reduction of TiO_2 at high temperature. And, the Vanadium promoted on Pt/ CeO_2 found new purpose and challenges due to its application in clean power generation systems. That found VO_x species were generated onto the catalysts by the different vanadium loading. The water gas shift kinetic reaction was associated with V-O-Ce bond. While, Hung, 2008 found the Bimetallic CuO/CeO_2 achieved to oxidize the ammonia to nitrogen by selective catalytic oxidation (NH_3 -SCO) between 423 and 673K. The electronic structure of system consists of various defect levels inside band gap, which plays a great role in silicon crystallization. And, the CeO_2 was implicated in water gas shift reaction e.g. Pt/ CeO_2 catalysts for low temperature water gas shift reaction (Jacobs *et al.*, 2002).

Accordingly, the Au/ CeO_2 was favoritely used in the low temperature water gas shift reaction. Chen *et al.* (2008) was examined the redox and formate mechanisms for water gas shift reaction on Au/ CeO_2 using density functional theory. They verified the two mechanisms over the water gas shift reaction that was redox and formate by CeO_2 behavior. The reaction occurring agree with El-Moemen *et al.* (2008). They found the high temperature was increased the reaction mechanism for

all catalysts. The catalysts were mainly deactivated by the formation of stable monodentate surface carbonates during the water gas shift reaction.

Ceramic membrane

Ceramic membranes usually consist of several composited layers of one or more different ceramic materials. They generally have a macroporous support, one or two mesoporous intermediate layers and a microporous or a dense at top layer.

Sol-Gel technique

Sol–Gel technology has a long history, starting with processing of oxide materials including glasses and ceramics about 30 years ago. However, since then, the technology has been employed in preparation not only of oxides, but also of non-oxide materials including nitrides, carbides, fluorides, and sulfides as well as oxynitride and oxycarbide glasses. It is a wet chemical route to synthesize a colloidal solid suspension particles or clusters in a liquid as sol (Bae, 2008) and dual phase forming with a solvent as gel, subsequently. The wet gel is converted to a xerogel at the ambient pressure drying when the solvent is removed.

However, recently sol–gel processing of mesoporous and macroporous materials has been attracted much attention, in synthesis materials with well-controlled pore characteristics and highly porous materials. Sol-gel processing allows high purity, high homogeneity nanoscale materials to be synthesized at lower temperatures compared to competing high-temperature methods (Theodore and Kunz, 2005). A significant advantage that sol-gel science affords over more conventional materials-processing routes is the mild conditions employed.

Two main routes and chemical classes of precursors have been used for sol-gel processing (Theodore and Kunz, 2005).

1. Colloidal route (inorganic route), which uses metal salts in aqueous solution e.g. chloride, oxychloride, nitrate as raw materials. These are generally low

cost and easier handle than the metal-organic route. However, their reactions were more difficultly for controlling the surfactant that required by that process might interfere later in downstream manufacturing and final utilization.

2. Alkoxide route (metal-organic route) in organic solvents. This route typically employs metal alkoxides $M(OR)_Z$ as the starting materials, where M is Si, Ti, Zr, Al, Sn, or Ce; OR is an alkoxy group; and Z is the valence or the oxidation state of the metal. Metal alkoxides are preferred because of their commercial availability and the high ability of the M-OR bond. They are available for nearly all elements and cost-effective methods. A larger range of mixed-metal nanoparticles can be produced under mild conditions, often at room temperature, by mixing metal alkoxides (or Oxoalkoxies) and other oxide precursors.

In general, the sol-gel process consists of the following steps: sol formation, gelling, shape forming, drying and densification. First, after mixing the reactants, the organic or inorganic precursors undergo two chemical reactions: hydrolysis and condensation polymerization, typically with an acid or base as a catalyst, to form small solid particles or clusters in a liquid (either an organic or aqueous solvent). Sol-Gel process is presented in Figure 6.

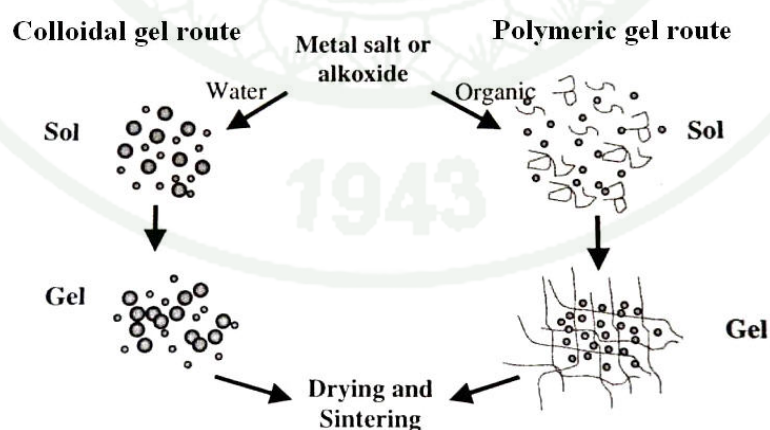


Figure 6 Sol-gel process

Source: Li (2007)

The resulting solid particles or clusters are so small (1 to 1,000 nm) that gravitational force is negligible and interactions are dominated by van der Waals, columbic, and steric forces. These sols, colloidal suspensions of oxide particles, are stabilized by an electric double layer, or steric repulsion, or a combination of both. The colloidal particles then link together by further condensation and a dimensional network occurs. As gelling proceeds, the viscosity of the solution increases dramatically.

The chemistry of the sol-gel process (Klein, 1991) can be simplified to:

Hydrolysis



Condensation-Polymerization



This circumstance makes metal alkoxides the most common candidates for the role of molecular precursors. The synthesis method of monometallic precursors is reacted on metals with alcohols as direct reaction in inert atmosphere. The sol-gel can be formed into three different shapes: thin film, fiber, and bulk. Thin (100 nm or so) uniform and crack-free films can readily be formed on various materials by lowering, dipping, spinning, or spray coating techniques. Sol-gel chemistry is promising, yet it is still in its infancy and a better understanding of the basic inorganic polymerization chemistry has to be reached. Some drawbacks include the high cost for the majority of alkoxide precursors, relatively long processing times, and high sensitivity to atmospheric conditions. Moreover, the batch nature of present sol-gel processing leaves cost and scale-up issues associated with the development of viable continuous production routes.

Sol-gel synthesis is an attractive catalyst preparation method for supported noble metal catalysts. This method can be used to produce catalysts with uniform metal distribution, tuneable particle size, high surface area, and uniform dispersion. The technique is based on the hydrolysis of precursors, mostly metal or semi-metal alkoxide. These fundamental chemical processes are influenced by several parameters which control the homogeneity and microstructure of the derived material.

Sol-Gel was used to fabricate the metal oxide for many applications. Silica glass (Arujo *et al.*, 1994) was generated the porous type-VI that was densification porous silica matrices. These glasses were produced for fully dense optical lens elements and micro-optic devices. The composite silica membranes were prepared for separation properties (Bai *et al.*, 1995). They were prepared by an in situ zeolite synthesis method using an alumina membrane tube with a 5 nm pore diameter. Transport through the membranes was controlled by molecular size and adsorption properties. The high separation factors were obtained with a pressure drop across the membranes. The alumina membranes themselves exhibited permeances expected for Knudsen or Knudsen plus surface diffusion. Moreover, the activated-gamma alumina sphere was used for macroporous porous (Faria *et al.*, 2008). The macroporous adsorbent was used by adsorption of Cd, Cu and As in the fixed bed adsorption columns. The adsorption test suggested that the spheres alumina powder had a great affinity.

Aluminium oxide (Al_2O_3)

Aluminium oxide (Alumina, Al_2O_3) is an amphoteric oxide of aluminium. It is an electrical insulator but has a relatively high thermal conductivity ($40 \text{ W m}^{-1} \text{ K}^{-1}$) for a ceramic material. Al_2O_3 is accountable for resistance of metallic aluminium to weathering. Metallic aluminium is very reactive with atmospheric oxygen, and a thin passivation layer of alumina (4 nm thickness) forms in about 100 picoseconds on any exposed aluminium surface. This layer protects the metal from further oxidation. The alumina generated by anodising is typically amorphous, but discharge assisted

oxidation processes such as plasma electrolytic oxidation result in a significant proportion of crystalline alumina in the coating, enhancing its hardness. The major uses of specialty aluminium oxides are in refractories, ceramics, and polishing and abrasive applications. Large tonnages are also used in the manufacture of zeolites, coating titania pigments, and as a fire retardant/smoke suppressant. Alumina is a medium for chemical chromatography, available in basic (pH 9.5), acidic (pH 4.5 when in water) and neutral formulations.

Alumina by sol-gel process was referred by many researchers. These were studied by different techniques process. The perovskite alumina was used as the ceramic membrane which was prepared from secondary-butoxide (Ahmad *et al.*, 2005). The PVA was added drop wise for modified the surface craterfield after calcinations at the high temperature. The sintering effect was studied by Ruhi *et al.*, 2007. They found that the sintering was an effect to corrosion and wear properties of sol-gel alumina coating on surface pre-treated mild steel. The increasing sintering temperature beyond 400°C appeared the detrimental towards the corrosion and wear performance of the coating. At 500°C it exhibited a very poor corrosion and wear resistance that was nearly bare metal substrate. The structural of alumina silica mixed oxide gel was also studied observation by sol-gel process (Peterlik *et al.*, 2007). The development of the structure of silica/alumina gel was investigated by small angle X-ray scattering through all stages of the preparation processes. Two processes were compared by the same precursor in 3-oxoethyl-6-trimethoxysilyl-hexan-2-one (OTH-H) with $\text{Al}(\text{OBu})_3$ and hydrodeacylation of OTH-H. Both processes occurred concomitantly at the beginning of the aggregation process and cluster-cluster aggregation dominated for opening the particle network.

MATERIALS AND METHODS

The materials were chemicals used in this study. The methods revealed the preparation method, material characterization, and the catalytic performance test. The details are displayed as follows:

Materials

1. Gold colloid (HAuCl_4), 0.01%, Sigma-Aldrich
2. Cerium nitrate hexahydrate ($\text{Ce}(\text{NO}_3)_3 \cdot 6\text{H}_2\text{O}$), 99%, Sigma-Aldrich
3. Polyvinyl alcohol (MW = 30,000-70,000), 95%, Sigma-Aldrich
4. Aluminum tri-sec butoxide (ASB), 95%, Fluka
5. Acetylacetone (ACAC), 95%, Carlo erba
6. Butyl alcohol (i- Butanol), 99.5%, Fisher chemical
7. Propyl alcohol (i-Propanol), 99.5%, Fisher chemical
8. Hydrogen gas (H_2), 99.99%, Thai Industrial Gases Public Company Limited
9. Carbon dioxide gas (CO_2), 99%, Thai Industrial Gases Public Company Limited
10. Carbon monoxide gas (CO), 99.2%, Thai Industrial Gases Public Company Limited
11. Steam (H_2O)
12. Nitrogen gas (N_2), 99%, Thai Industrial Gases Public Company Limited
13. Helium (He), 99.99%, Thai Industrial Gases Public Company Limited
14. High voltage (Electrospinning apparatus), Gamma high voltage, ES20P-20W
15. Stationary collector module, aluminum foil plate
16. Alumina disk diameter 38.1 mm and thickness 1 mm, 46% porosity
17. Viscometer, Brookfield, Model DV-II+
18. Simultaneous DSC-TGA Analyzer, TA Instruments, Model SDT 2960
19. X-ray diffractometer, Phillips, Model PW1830/40
20. Scanning electron microscope, JEOL, Model JSM 5600 LV
21. Autosorb-1C, Quantachrome

22. Gas Chromatography (GC), Shimadzu, Model GC-2014
23. Fixed bed reactor (In-house made)
24. Catalytic membrane reactor (In-house made)
25. Mass flow controller, Aalborg, Model GFC17
26. Glass wool

Methods

The main procedure in the experimental plan was divided into two parts: (1) fabrication of catalytic reactor and (2) testing the performance of the reactor for the water gas shift reaction. The work flow diagram is shown in Figure 7.

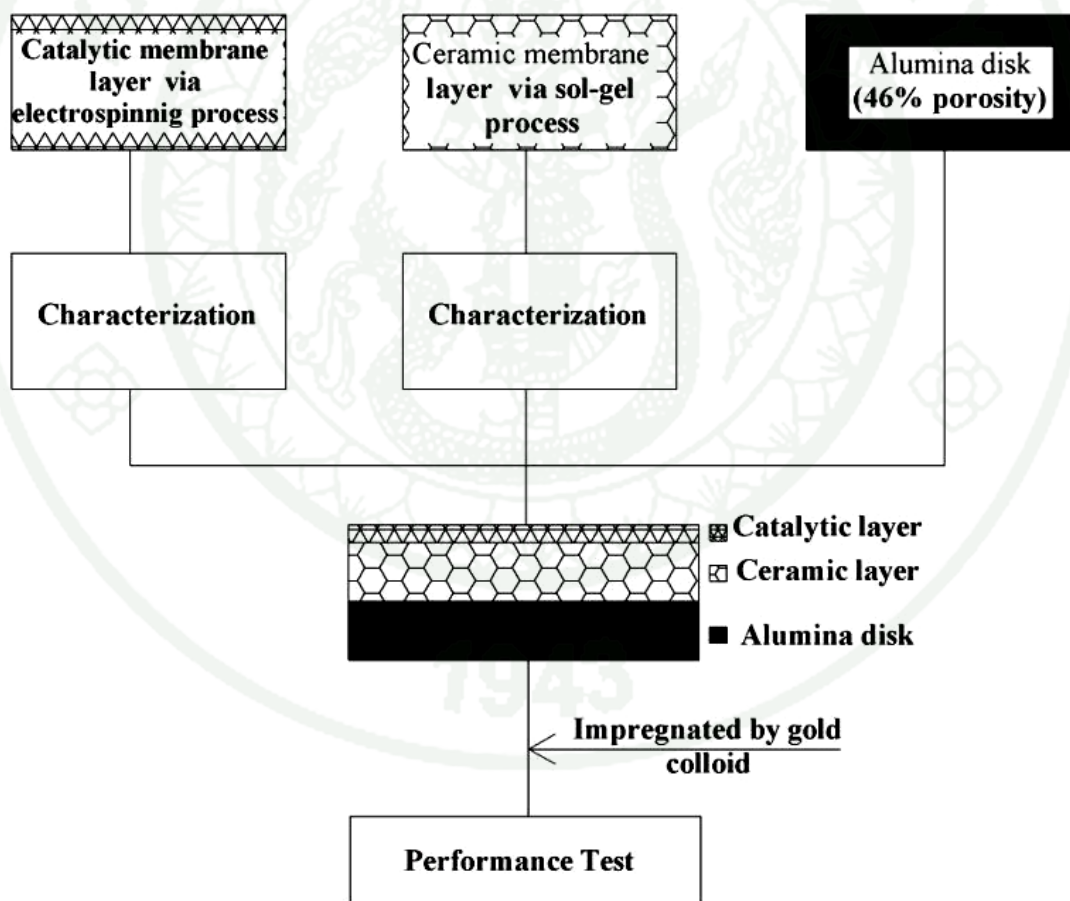


Figure 7 Flow diagram of this work

1. Experimental preparation

Catalytic membranes reactor is a novel technique in the recent day. The application is selectively. The layers usually consists the composite materials by ones consisting of several layers. They generally have a macroporous support, one or two mesoporous intermediate layers and a microporous or a dense at top layer. The topped layer should be catalytic for the reactivity.

1.1 Preparation of catalytic membrane layer

Cerium (III) nitrate hexahydrate ($\text{Ce}(\text{NO}_3)_3 \cdot 6\text{H}_2\text{O}$), polyvinyl alcohol (PVA, $(\text{CH}_2\text{CHOH})_n$), and iso-propanol ($(\text{CH}_3)_2\text{CHOH}$) were used without further purification. Cerium nitrate (1.0 M) was dissolved and stirred continuously in a co-solvent of water and i-propanol. The investigated factor was wt% of i-propanol in the co-solvent. Initially, 0 wt% of i-propanol was observed then stepping up to 10, 30, and 50 wt%, respectively. Then, 20 % w/w of PVA was slowly added into the precursor solution and stirred vigorously until viscous and clear solution was obtained.

1.1.1 The electrospinning process setup

The high voltage power supply and the distance between a metal needle tip and a ground collector were significant studied variables. The correct conditions will give the high quality of electrospun fibers, which are smooth line and continuous. The electrospinning process was set up as shown in Figure 8. The experimental was started up by pouring the co-solvent solution into a glass syringe with a 2 mm diameter metal needle. Then, the high voltage power was supplied across the needle tip and the grounded collector.

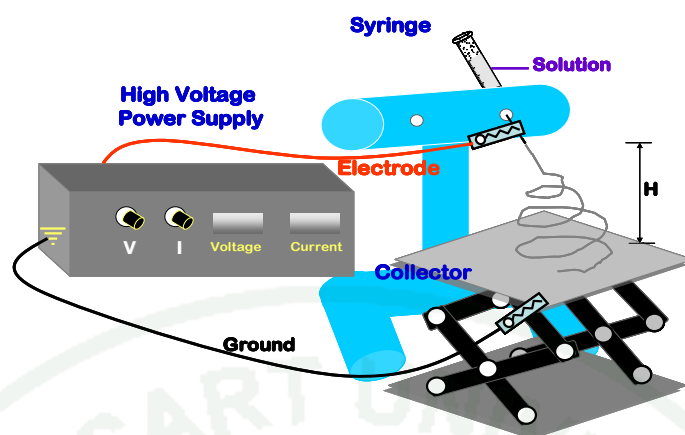


Figure 8. Electrospinning equipment set up

Firstly, the 6 kV of electrical field was applied with 7 cm distance. The electrospun fibers were ejected in a web form onto the aluminum ground collector. Later, the electrical fields were varied to 9, 12, 15, and 18 kV, respectively. The smooth and continuous electrospun fibers at any electrical field were chosen for further work. Further, the distance was a latter parameter. For selected electrical field the distance between needle tip and collector was varied at 6, 7, 8, 9, and 10 cm. The optimum electrical field and distance was then selected for further study.

1.1.3 The mixing solution behavior

Thermal gravimetric analysis was used to measure the weight loss of sample prepared. The result was used to select the appropriate calcinating temperature. The sample was heated at the rate of 10°C/min under 100 ml/min of nitrogen.

1.1.4 The identification of synthesis fibers

Finally, the acceptance data would be express to electrospun fibers. The fibers morphology was analyzed by a scanning electron microscopy (SEM) and the chemical composition of the fabricated electrospun fibers was

determined using energy dispersion X-ray analysis (EDX). The crystal structure of the obtained product was analyzed using X-ray powder diffractometer (XRD).

1.2 Preparation of ceramic membrane layer

The starting chemicals were aluminum tri-sec butoxide, iso-butanol, and acetylacetone (ACAC) used without further purification. The investigated parameters were the average pore size, the surface area, the pore volume, and the size distribution of synthesized alumina

1.2.1 Effect of water/alkoxide ratio

Firstly, 12 moles iso-butanol was adding into 1 mole Aluminum tri-sec butoxide and continuous stirring for 3 hour at room temperature under N_2 atmosphere. Then, the 5 mole of distilled water was slowly adding into the clear solution until the gel formed. The gel was kept under atmosphere for 2 days and then sintered at $800^{\circ}C$ for 3 hours. The experiment was repeated with water concentration at 10, 15, 20, 25, 30, 35, 40, and 45, respectively. The obtained product was determined pore size and its distribution by N_2 adsorption.

1.2.2 Effect of ACAC concentration

12 mole iso-butanol was added into 1 mole Aluminum tri-sec butoxide and continuously stirred for 1 hour at room temperature under N_2 atmosphere. Then, ACAC was added drop wise into the solution. The solution was stirred for another 2 hours at the same condition. Then, the water slowly added into the mixed clear solution until the gel formation. The gel was kept under atmosphere for 2 days and sintered at $800^{\circ}C$ for 3 hours. The various concentrations of ACAC were examined. The ACAC amount was varied at 0.2, 0.3, and 0.4 mole.

1.2.3 Effect of sintering process

In order to control the pore size and pore distribution of the prepared samples, sintering at different temperature (500 – 1000°C) was applied to the samples for 3 hours. At 1000°C the sintering time was varied at 1, 3, and 5 hours. Subsequently, the sintered sample was measures the pore size and its distribution.

1.2.4 Gas interaction study

The interaction between alumina layer and corresponding gas (i.e. CO, CO₂, H₂) was investigated by a single gas adsorption experiment. First, the alumina gel was spin-coated on the alumina supporting disk. Then it was dried and calcined at suitable condition obtained from previous section. The spin-coat was repeated 3 times totally. The final thickness of the fabricated layer was about 0.1 mm. The disk was placed inside the testing module (Figure 9). The gas interaction was operating under atmospheric pressure at 250°C for 30 minutes. The gas flowrate was 20 ml/min. The studied gases were CO, CO₂, and H₂. The inlet gas concentrations were 23.1, 16.6, and 16.0 µmol, respectively. The outlet gas effluents were analyzed using a gas chromatography.

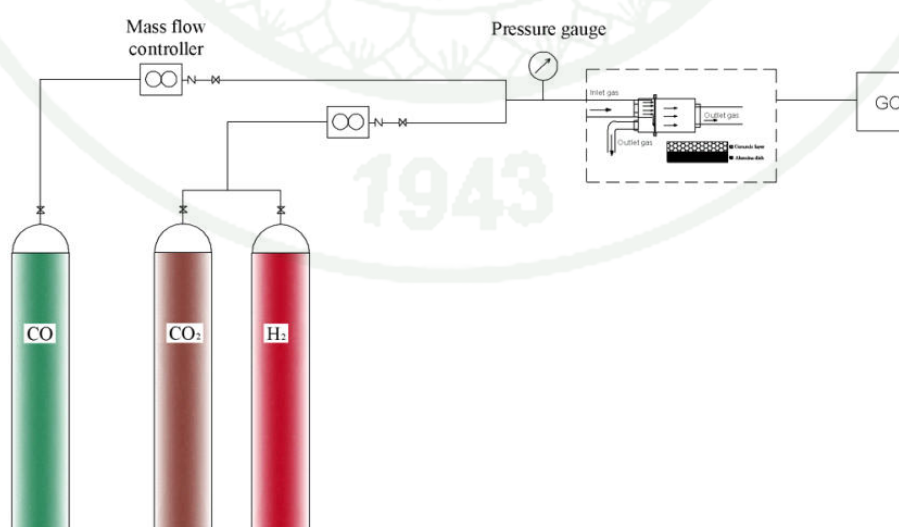


Figure 9 Gas interaction performance set up

The adsorption between supplied gas and alumina disk was then calculated by following equation(Wittayakhun *et al*, 2004):

$$\% \text{ Adsorption} = \frac{[\text{Gas}]_{\text{inlet}} - [\text{Gas}]_{\text{outlet}}}{[\text{Gas}]_{\text{inlet}}} \times 100 \quad (10)$$

2. Characterization

2.1 Viscosity

The viscosity of the co-solvent solution having different i-propanol:water ratio was determined by Rheometer Brookfield, Model DV-II at the Faculty of Industrial Textiles and Fashion Design, Rajamangala University of Technology Phra Nakhon. The measurement was conducted at the room temperature.

2.2 Crystal structure

Crystal structure of obtained electrospun product was determined by X-ray powder diffractometer (XRD, Phillips PW 1830/40) at the Department of Material Engineering, Faculty of Engineering, Kasetsart University. The XRD spectrum were recorded on a Multiflex X-ray diffractometer using Cu-K α 1 radiation with $\lambda = 1.5406 \text{ \AA}$ at 40 kilovolts tube voltage and 40 mA tube current with a scanning speed of $0.01^\circ/\text{min}$ in the range $0-90^\circ$ (2θ). The XRD patterns were referenced to the powder diffraction file JCPDS-81-0792 (International Centre for Diffraction Data) for identification.

2.3 Pore size and pore size distribution

The N₂ adsorption-desorption isotherms of catalysts were measured on Autosorb-1C, Quantachrome instrument at the Department of Chemical Engineering, the Faculty of Engineering, Kasetsart University. It was used to determine synthesized alumina. All samples were evacuated at 120°C for removing adsorbed

H₂O from the surface prior to analysis. The specific surface area was calculated using Brunauer-Emmett-Teller (BET) method at 39, and 55 points N₂ adsorption/desorption. The total pore volume was determined at a relative pressure $P/P_0 = 0.99$. Pore size distribution were calculated from the desorption isotherms using the Barrett, Joyner, and Halenda (BJH) method. The desorption leg of the isotherm is preferred for pore analysis since it is thermodynamically more stable than the adsorption leg due to the lower Gibbs free energy change.

2.4 Fiber morphology

Scanning electron microscopy (SEM) was taken for three-dimensional appearance surface structure of the materials, shapes and particle sizes. It also identified for spot elemental analysis with energy dispersive X-ray spectroscopy (EDS). The powder sample was sprinkled on a carbon sticky tab of aluminum specimen mount and coated with a nanometer-thick layer of gold (Au) using a sputter coater before being examined and photographs SEMs. In this studied, Hitachi S-510 with 20-30 kV energy at Department of Medical Science, Ministry of Public Health, and Phillips JEOL, JSM-5600 LV with 15-20 kV energy at Department of Material Engineering, Faculty of Engineering, Kasetsart University for determined the morphology of synthesis ceria electrospun fibers. And, Phillips JEOL, JSM-5600 LV with 15-20 kV energy, energy dispersion X-ray analysis (EDX; EDAX Falcon, EDAX Co. Ltd., NJ) and the Edward Scancoat six sputter coater (Edwards Laboratories, Milpitas, CA) for sputtering Au at the Department of Material Engineering, Faculty of Engineering, Kasetsart University were used to analyze the elements on synthesized ceria fibers.

2.5 Calcination temperature

Differential thermal and thermogravimetric analyses (DTA/TGA Analyzer SDT 2960 Universal 2000) were performed on two samples. These were polyvinyl alcohol and mixed polyvinyl alcohol and cerium nitrate hexahydrate in co-solvent. It was used to examine the thermal and gravimetric changes that occur in

those samples during calcinations. The samples were heated under air flow from room temperature to 600 °C at heating rate 20°C/min. The material structure analysis was performed at the Department of Chemical Engineering, Faculty of Engineering, Kasetsart University.

2.6 Analysis the gas compound

The gas permeability and reaction performance of conversional reaction were determined by Gas chromatography (Shimadzu GC-2014) at the Department of Chemical Engineering, Faculty of Engineering, Kasetsart University. The Gas chromatography was operated by TCD detector and Unibead C Column. The operating condition was 25 kPa (0.25 kg/cm²) for the whole gas in the system as tested gas, and Helium gas. The operating temperature was 100°C. The inlet temperature was 100°C, and the outlet temperature was 150°C. The electricity currency was 100 mA, at 512 signals.

3. Layer integration

The CeO₂ electrospun fibers as a catalytic membrane layer were covered on ceramic membrane layer. The gold colloid was impregnated into catalytic layer. The integrated model is illustrated in Figure 10.



Figure 10 Catalytic membrane composition

4. Water gas shift reaction performance

The performance of the reactor was examined at the atmosphere pressure. The investigated parameters were the comparative performance among catalytic

membrane reactor, packed bed reactor, and hybrid membrane reactor. The reactors set up are shown in Figure 11.

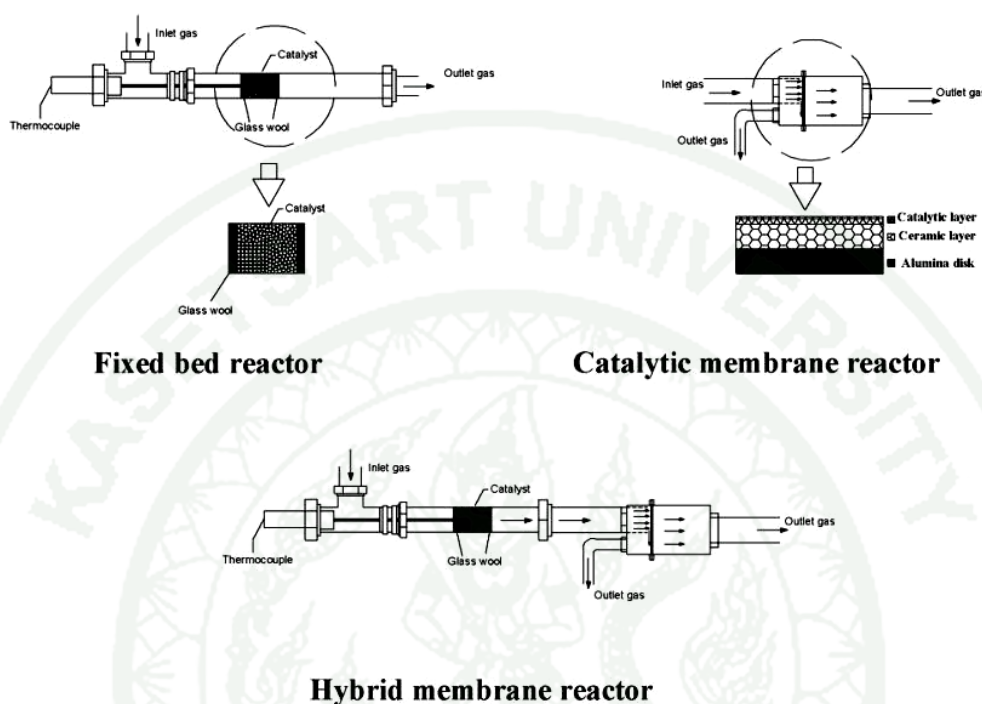


Figure 11 Reactor types in this study

The reactions were tested in all the reactors at atmospheric pressure. They were conducted at temperature 225, 250, 275°C for 15, 45, and 75 minute, respectively. The CO velocity at the inlet was 20 ml/min. The inlet CO concentration was 8.22 μmol and the exceed H_2O was accessed. The each reaction runs were done by 0.34 gram CeO_2 as the catalyst. The catalysts were impregnated with 0.01% HAuCl_4 and reduced in flowing H_2 for 30 minutes at 250°C before starting reaction. The outlet gas concentrations were analyzed using a gas chromatography. For the fixed bed reactor and the hybrid membrane reactor glass wool was inserted into the tube to prevent catalyst loss. The schematic diagram of the water gas shift reaction is shown in Figure 12.

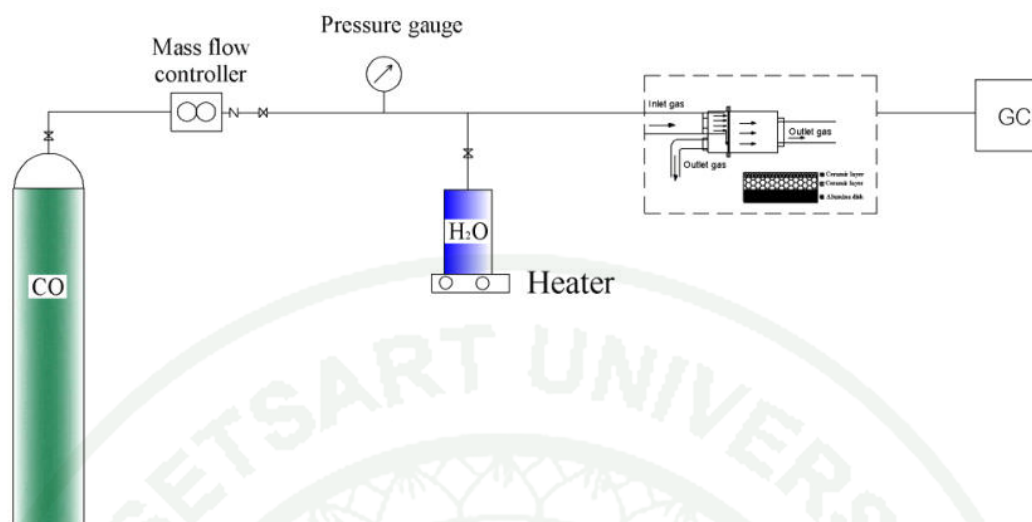


Figure 12 Schematic diagram of water gas shift reaction

Subsequently, the water gas shift reaction performance was evaluated in term of CO Conversion (X_{CO}). The conversion was calculated by following equation (Park *et al.*, 2000) :

$$X_{CO} = \frac{[CO]_{inlet} - [CO]_{outlet}}{[CO]_{inlet}} \times 100 \quad (11)$$

RESULTS AND DISCUSSION

1. Preparation of catalytic membrane layer

The catalytic membrane layer was the top layer of the composite membrane layer. It was designed to act as an active layer for the water gas shift reaction. This layer was fabricated by electro-spinning process. The investigated parameters were viscosity, the applied voltage for spinning process, distance between tip and a ground collector, calcination temperature. The results are reported and discussed as follows:

1.1 Effect of co-solvent

The co-solvent is a solution that is added into a mixture as another solvent. The mixed solvent becomes greatly enhancing the solvent power due to their synergism. In this study, i-propanol was used altogether with water forming a mixed solvent for dissolving $\text{Ce}(\text{NO}_3)_3$ and PVA. The varying i-propanol was 0, 10, 20, 30, 40, and 50 wt %, respectively. The viscosity of the mixture was measured and presented in Table 1.

Table 1 The effect of i-propanol on solution viscosity

i-propanol (wt.%)	Viscosity (Pa.s)
0	1
10	10.8
30	20.7
50	50.5

From Table 1, it is clearly seen that the wt% i-propanol impacted on the solution viscosity. The solution viscosity was increased when increasing i-propanol

in the electrospinning process, the property of the solution played a significant role in the fiber morphology. The key properties were surface tension, polymer solubility, and viscosity. The co-solvent solution viscosity depends on the PVA solubility which can be explained by the dielectric constant of a solvent. The dielectric constant is a relative measure of polarity. Water has a dielectric constant of 80 (high polarity), while i-propanol has a dielectric constant of 20 (semi-polar), and PVA has a dielectric constant of 2 (low polarity) at 20°C (Clipper Controls Inc., 2005). This implies that PVA can be dissolved in i-propanol better than in water. There are two stages when a polymer dissolved in the solvent (Ramakrishna *et al.*, 2005). Firstly, solvent molecules diffused slowly into the polymer bulk to produce a swollen gel. Secondly, the polymer bonds are broken forming true solution. Thus, the addition of i-propanol as the co-solvent will enhance the solubility of the PVA and increase the viscosity of the solution as shown in Table 1. However, if the viscosity is too high, it will be very difficult to draw the fibers due to the cohesion effect on the metal needle tip. Hence, the 50 wt% i-propanol was an appropriated mixing solution and was chosen for further electrospinning processes.

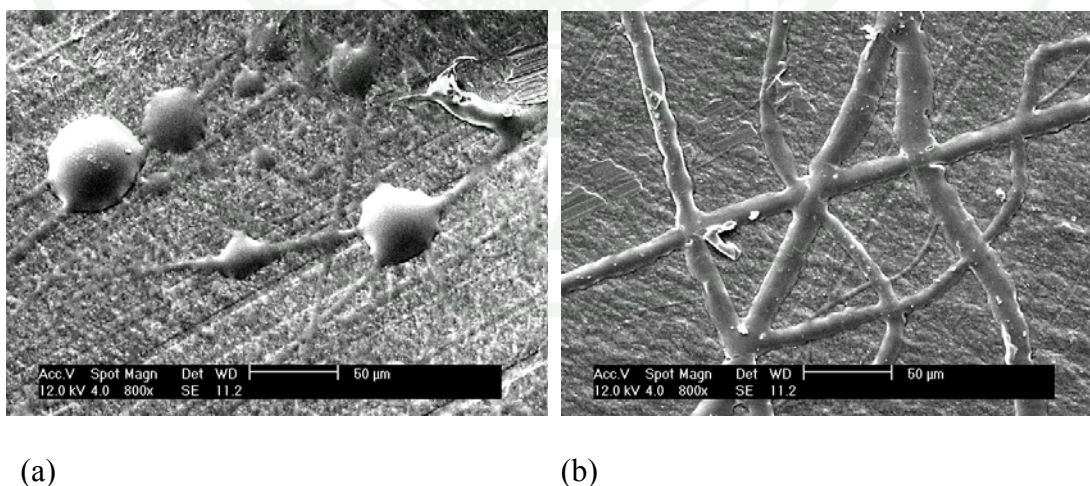
1.2 The effect of applied voltage

A high voltage is a crucial element in the electrospinning process. It will induce the necessary charge on the solution and together with the external electric field. The electrostatic force must be high enough to overcome the surface tension of the solution. Generally, the high voltage is able to cause the solution drop to distort into the shape of a Taylor cone when the electrostatic force in the solution overcomes the surface tension of the solution. An external electric field is used to control the charged electrospinning jet. In this study, the voltage applied was varied from 6 – 18 kilovolts at across the needle tip and ground collector which was set to be 7 centimeters. The morphology of the obtained product is summarized in Table 2.

Table 2 The fiber morphology at the different electric field

Power supply (kV)	Morphology
6	Discontinuous fiber, spherical shape on the fiber (Figure 13 a)
9	Discontinuous fiber, spindle shape, and bead on the fiber
12	Continuous fiber, almost spherical shape, and medium scale bead on the fiber
15	Continuous fiber, spherical shape, and small scale bead on the fiber
18	Continuous fiber, cylindrical shape as smooth line, and no bead on the fiber (Figure 13 b)

Generally, the interaction between the solution and the charges on the jet will determine the fiber distributions in the process. Since, the high voltage was applying in the process. When the applied voltage was increased, the polymer jet was accelerated faster and more solution volume.

**Figure 13** Electrospun fiber obtained at 6 kV (a) and 18 kV (b)

At the low voltage, the electrostatic force was not higher than the surface tension of the solution then the solution drop was not distorted into the Taylor cone and remained as a drop as seen in Figure 13 a). In this case, an electrospray was occurred instead of electrospin. In most cases, a higher voltage will lead to greater stretching of the solution due to the greater columbic force jet. It was also reported that the shape of the beads would be changed from spherical shape to spindle shape when increasing voltage as seen as Figure 13 b). Moreover, the increased stretching of the jet due to higher voltage would inhibit bead formation. Therefore, for this study the 18 kV was selected for fabrication of the catalytic layer.

1.3 The effect of distance between tip and collector

The distance between tip and collector will directly affect on the flight time and the electric field strength. The length is a direct influence in both the flight time and the electric field strength. The electospun jet must have enough time for evaporating its solvents. This factor is a key role that controls the obtained fiber diameter. In this study, the distance was varied from 6 to 10 cm at 18 kV electrical field. The results are shown in Table 3 and Figure 14-15.

Table 3 The morphology fiber at the different distance

Length (cm)	Morphology
6	Merged fibers, and un calculated fiber diameter, (Figure 14)
7	A few merged fibers, and un calculated fiber diameter
8	Continuous fibers, no bead on the fibers, and average diameter as 900 nm (Figure 15)
9	Uncontinuous fibers, no bead on the fibers, and average diameter as 900 nm
10	No fiber on the collector

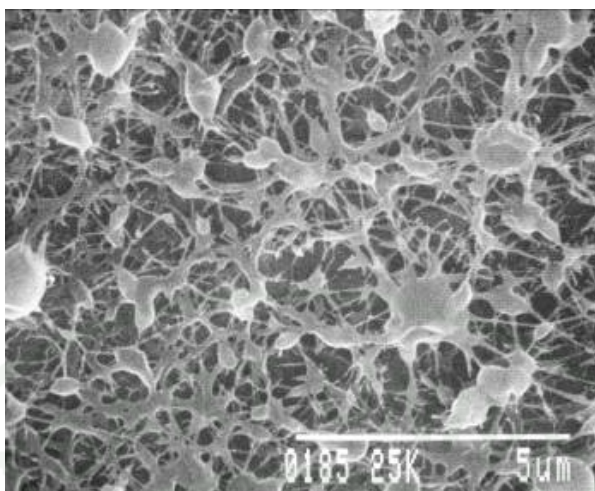


Figure 14 Merged fiber obtained at 6 cm

At 6 cm, the time was not enough for drawing setting therefore the fibers were connected by accumulated solvent as seen as Figure 14. Moreover, the electrospun fibers were obtained at the higher distance but the fiber diameters become smaller when the distance was increased. However, for too long distance the spun fibers did not fall on the collector, which is in agreed with Zhao *et al.*, 2006. The greater elongation force on the electrospinning jet caused by the more mobile smaller ions could yield fibers with smaller diameter. Conclusively, 8 cm distance and 18 kV electric field were chosen for making ceria fibers.

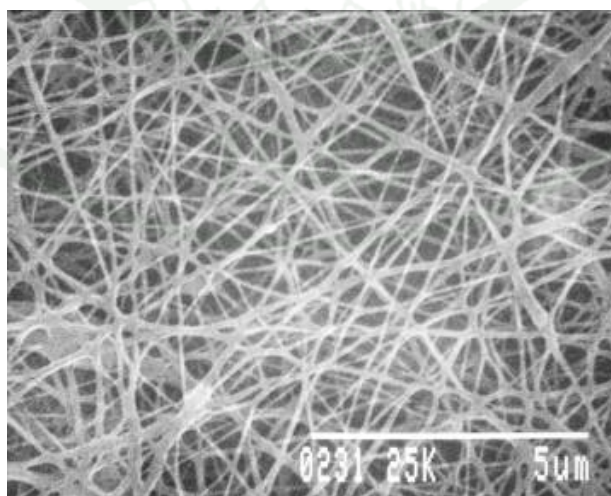
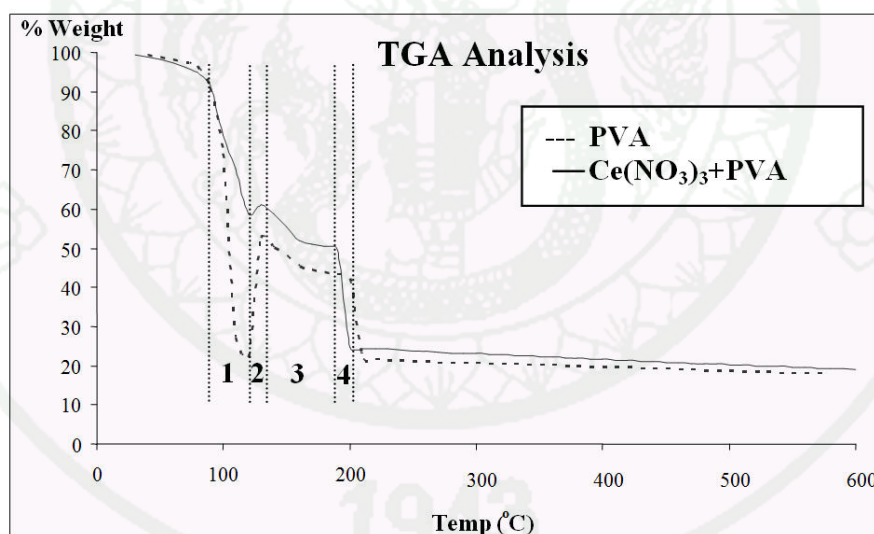


Figure 15 SEM micrograph at 18 kV and 8 cm distance

Figure 15 shows the electrospun fibers prepared with the selected conditions. The fibers diameter is 900 ± 250 nm (S.D. = 90) determined by an image analyzer. This formation could be attributed to the reduction of surface tension of the solution resulting from adding i-propanol. Because i-propanol had much lower surface tension than water as mentioned earlier, the more i-propanol was added into water, the lower surface tension of the mixture was achieved.

1.4 Thermal behavior of mixed solution

Since weight loss and gain are disruptive processes to the sample material or batch, knowledge of the magnitude and temperature range of those reactions are necessary in order to design adequate thermal ramps and holds during those critical reaction periods. In this study, the PVA, and $\text{Ce}(\text{NO}_3)_3$ + PVA in co-solvent was observed. The results are displayed in Figure 16.



Remark: Region 1 was a solvent effect, Region 2 was a solvent vaporization and polymerization effect, Region 3 was a polymerization behavior and solute degradation, and Region 4 was a remaining product.

Figure 16 Thermal behavior of the mixed solution

In Figure 16, the weight change can be classified into 4 regions representing vaporization of solvent, partial oxidation of PVA, degradation of PVA, and PVA and $\text{Ce}(\text{NO}_3)_3$ decomposition, respectively. In the region 1, the co-solvent was vaporized at its boiling point. In the region 2, the parts of PVA structure were cracked and subsequently reacted with oxygen forming intermediate substances resulting in weight gain. Then, at temperature above 130 °C, PVA started to be degraded gradually until reaching 200 °C. Finally at 190 °C, $\text{Ce}(\text{NO}_3)_3$ and PVA were decomposed abruptly to be CeO_2 and ash, respectively. It should be noted that pure PVA was decomposed at temperature slightly higher than $\text{Ce}(\text{NO}_3)_3$ +PVA (solid line). Although the decomposition is completed at 190°C, the calcinations was carried at 450°C in order to making the ceria fibrous layer strong enough for handling.

1.5 Fibers characterization

The fiber morphology is extremely useful for understanding the expected structure of components and quality of fiber. These are using the SEM which means that closely spaced features can be examined at a high magnification. The combination is highly magnification, larger depth of focus, greater resolution, and ease of sample observation. Also, SEM-EDX is the name of the energy-dispersive X-ray spectroscopy analysis conducted by means of SEM. It determines the element composition of a specimen. In this study, the synthesized fibers (before calcination and after calcination process) were examined. The results are presented in Figure 17 and Table 4, respectively.

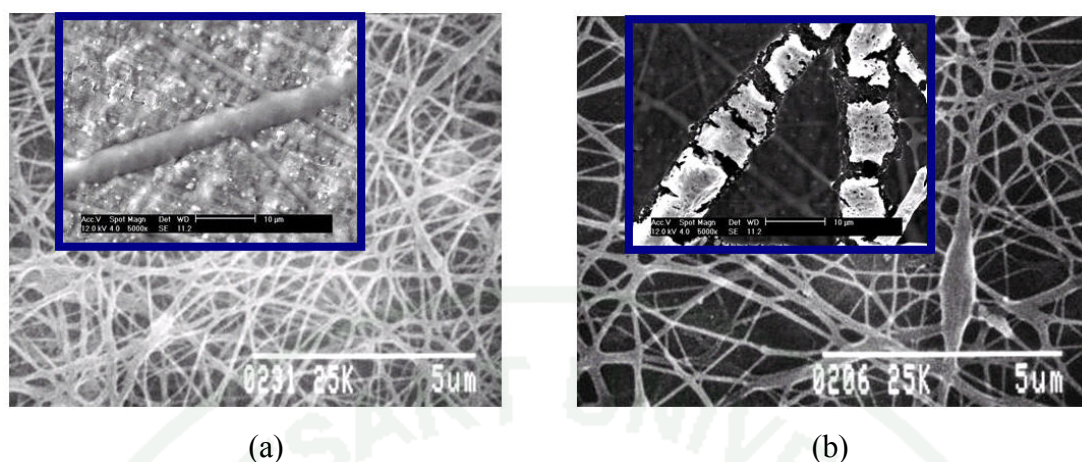


Figure 17 SEM micrographs of fibers before (a) and after (b) calcination

The fiber diameter was measured from the SEM image using an image analyzer software (Image J, Version 1.42). Before calcination, the obtained fibers had smooth surface having average diameter of 900 ± 250 nm (S.D. = 90). After calcination at 450°C for 3 hours, their surfaces were cracked resulting from the gases evolution during the PVA and $\text{Ce}(\text{NO}_3)_3$ decomposition and their sizes were shrunk to 630 ± 80 nm with narrower distribution (S.D.=29). The chemical compositions reported as element determined by EDX are shown in Table 4.

Table 4 Elemental composition on the fibers

State \ Element	C (%)	N (%)	O (%)	Ce (%)
Before calcination	18.44	19.48	55.29	6.79
After calcination	1.50	12.25	57.92	28.31

It reveals that before calcination the fiber comprised of $\text{Ce}(\text{NO}_3)_3$, PVA, and residual i-propanol. After calcination, the composition corresponds to CeO_2 , fixed carbon (ash) and unconverted cerium nitrate, which is in agreement with the TGA

analysis. Moreover, oxygen and cerium had the highest percentages. The calcination process was a heat treatment to effect phase transformations. It induced the calcination process that transformed the polyvinyl alcohol/cerium nitrate composite fibers to CeO_2 fibers. The percentages of cerium and oxygen were 28.31 and 57.92, respectively. The yield proportion was approximately 1:2 and there was a strong possibility that it was CeO_2 .

The XRD technique was used to verify the crystal structure of the polycrystalline phases. The obtained XRD pattern is shown in Figure 18.

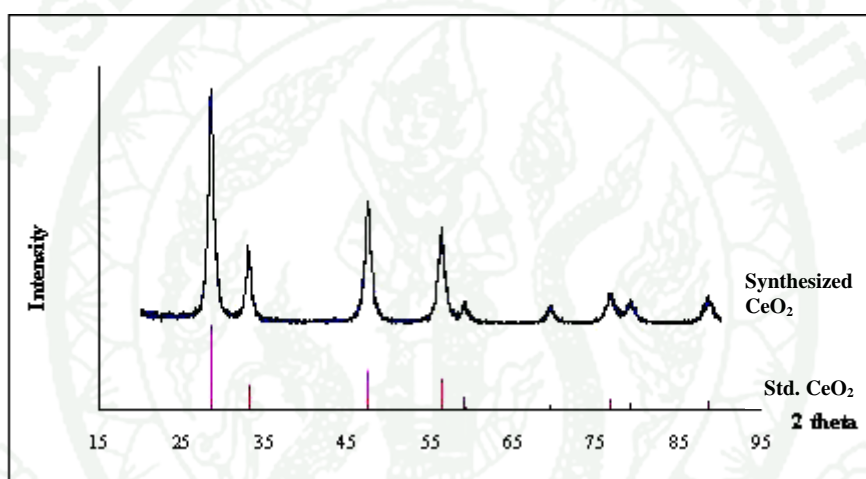


Figure 18 XRD pattern of synthesized fibers

The crystalline were arranged in position (2 θ) as 28.54, 33.08, 47.48, 56.33, 59.08, 69.40, 76.69, and 88.41. The pattern was matched well with the standard pattern of CeO_2 on International Centre for Diffraction Data (JCPDS) file number 81-0792. That means the calcined fibers were completely transformed to CeO_2 .

2. Preparation of alumina membrane layer

The alumina membrane layer was a middle layer of the catalytic membrane disk. It was designed to act as a separation layer for the water gas shift reaction. This layer was fabricated by sol-gel technique. The reaction was conducted under N_2 atmosphere. The results are reported and discussed as follows:

2.1 The effect of water/alkoxide ratio

In the sol-gel process, water is a reactant for hydrolysis reaction and also product from concentration polymerization. Adding different amount of water will affect the synthesized gel properties. In this study the molar ratio of water/alkoxide was increased from 10 to 45. After heat treatment at 800°C for 3 hours, the samples were analyzed by N₂ adsorption and results are summarized in Table 5.

Table 5 N₂-adsorption analysis of calcined alumina synthesized by using different molar ratio of water/alkoxide

ASB (mole)	H ₂ O (mole)	pore size (Å)	Surface Area (m ² /g)
1	10	307.4	222.8
1	15	175.3	207.7
1	20	175.2	212.6
1	25	174.1	208.9
1	30	123.8	152.2
1	35	65.6	157.2
1	40	49.0	302.4
1	45	49.0	305.4

From Table 5, the pore size from N₂-adsorption analysis on synthesized alumina particles was decreasing when the water/alkoxide ratio was increased. At low water/alkoxide ratio the condensation rate was faster than at high ratio because water acted as diluent. The gel network was quickly developed creating an extensive

network of branch chains. At the end, the looser gel was obtained having larger pore size with broader distribution and lower surface area as presented in Table 5.

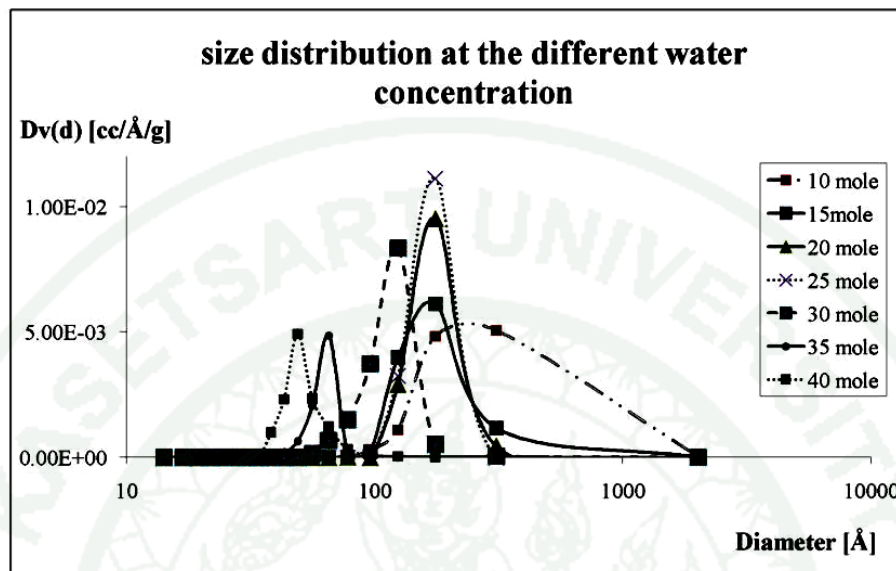


Figure 19 Size distribution by the different water concentration

Nevertheless, the products prepared by using 15-25 mole of water had almost the same pore sizes. However, when the pore distribution (Figure 19) was considered it is clearly seen that the lower water content yielded the broader pore size distribution and lower pore volume at the corresponding mean pore size. This is following the same trend as explained earlier. Consequently, the ratio of 40 mole was chosen for further experiment because it gave the smallest pore size and high surface area. For the ratio of 45, the membrane layer was unable to be formed.

2.2 The Effect of ACAC concentration

ACAC is an organic compound as ketone. It is a common bidentate ligand which it is building block for the synthesis of heterocyclic compounds. ACAC is also a significant chemical which impacted to the gel networking. In this study, ACAC was added drop wise into 1 mol ASB from 0.2 – 0.4 mole at 40 mole water. Then, the gel was treated at 800°C for 1 hour. The results are presented in Table 6.

Table 6 N₂-adsorption analysis of calcined alumina synthesized by using different molar ratio of ACAC

ASB (mole)	ACAC (mole)	H ₂ O (mole)	pore size (Å)	Surface Area (m ² /g)
1	0.2	40	65.5	163.2
1	0.3	40	65.6	157.2
1	0.4	40	65.5	178.3

By comparing the previous results, it was clearly seen that ACAC was an essential factor to reduce pore size of synthesized alumina by the manner characteristic. Namely, ACAC formed the complexes anions to the metal ions wherein both oxygen atoms bind to form six-member chelateting ring. That obstructed the performed high condensation polymer. The inner molecules had high rearrange time, they were hard structure whereas smaller orientation quantity.

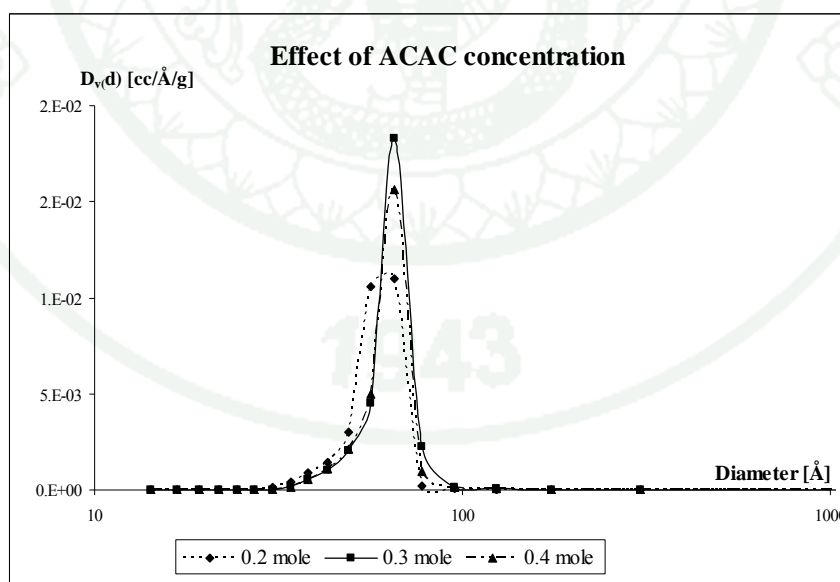


Figure 20 Size distribution of synthesized alumina by ACAC varying

However, the ACAC concentration seem the nearly almost properties in pore size, surface area whereas the size distributions were different. At 0.3 mol ACAC gave the narrowest distribution, so it was selected to be in the next study. The distribution is compared in Figure 20.

2.3 The sintering effect

Sintering is a method for powder production by temperatures The process was operated at the below its melting point until its particles adhere to each other. That is associated to a remarkable shrinkage of the material because glass phases flow and start powder consolidating in structure and porosity. In this study, the temperatures and time were investigated by 1 mole ASB, 0.3 mole ACAC, and 40 mole water. The first case, the temperature was increasing from 500 – 1000°C for 3 hour. The summarized results are presented in Table 7. The second case, sintering time was set up for 1-3 hours at 800°C. The results were summarized in Table 8.

Table 7 N₂-adsorption analysis at the different sintering temperature

Temp (°C)	pore size (Å)	Surface Area (m ² /g)
500	43.2	520.6
600	43.2	447.6
700	49.0	374.2
800	49.0	302.4
900	56.3	261.6
1000	65.6	170.7

While the temperature was increasing dramatically between 500 - 800°C, the grain size does not show a remarkable change. In contrast, the pore size was increasing as temperature excess from 800 - 1000°C. It indicated that coarse pores

have been developed at higher temperature than low temperature. The distribution is shown in Figure 21.

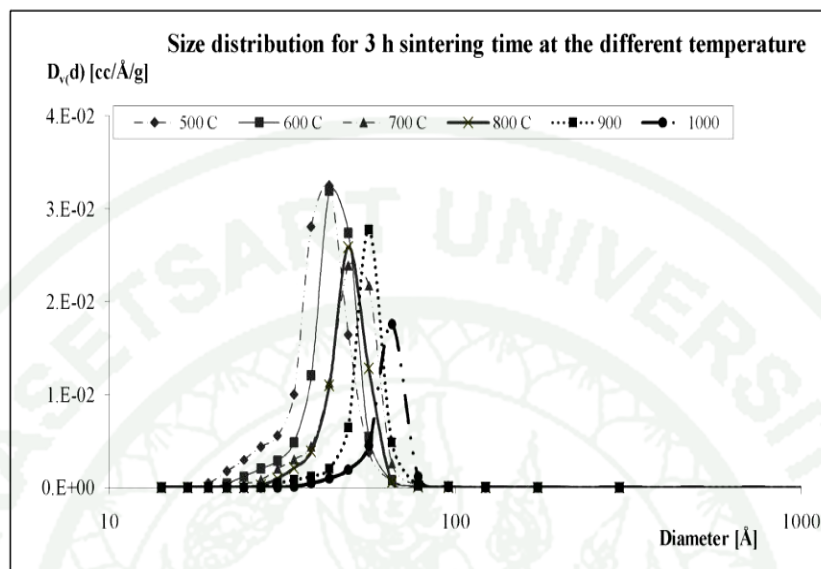


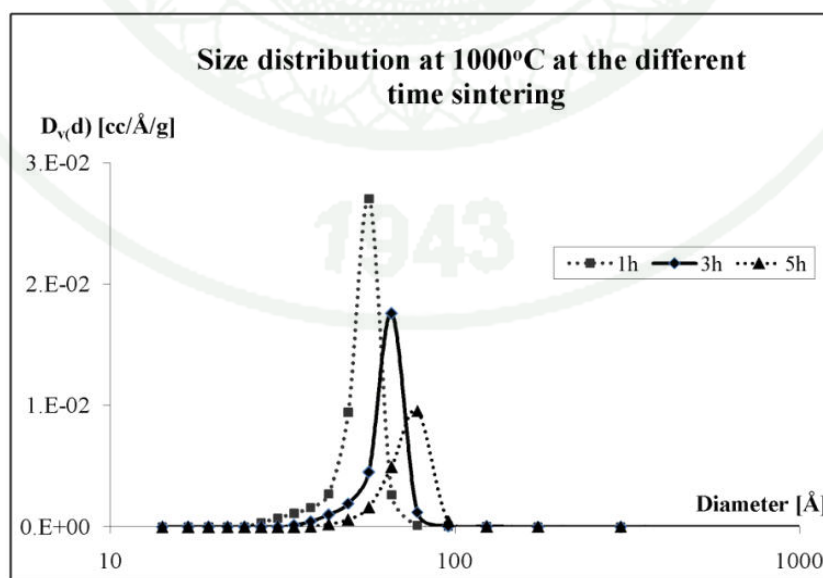
Figure 21 Size distribution by the different temperature sintering

At elevated temperatures the particles were able to bond together to form a fairly rigid structure which hinders the shrinkage of the wet gel to a densely packed dry gel. The larger pores tend to shrink more slowly than the smaller pores (Araujo *et al.*, 1994). These effects caused the dehydration on the surface of the sol particles. At the higher particle collision rates implied higher rates of bond formation through dehydration polycondensation. The coarsening ultimately dominated and leads to an incredible decline in sintering rate at the temperature above 850°C (Mazaheri *et al.*, 2008). Therefore, the coarse pores have been greater developed in the membrane at higher temperature than lower temperature (Ahmad *et al.*, 2005). For this study, at 500°C was accepted for further work.

Table 8 N₂-adsorption analysis at the different sintering time

Time (h)	pore size (Å)	Surface Area (m ² /g)
1	56.3	256.3
3	65.7	167.0
5	78.1	122.3

Furthermore, the time was a significant parameter in sintering process, also. The sintering occurs by diffusion of atoms through the microstructure. This diffusion is caused by a gradient of chemical potential – atoms move from an area of higher chemical potential to an area of lower chemical potential. The different paths the atoms take to get from one spot to another are the sintering mechanisms. As in Table 8, the time was not remarkable effect on pore size properties but the shorter time would reduce shrinkage surface area during drying. Since, atoms from surface diffuse through lattice and rearrange them onto another surface or part of the same surface. These mechanisms simply rearrange matter inside of porosity and did not cause the shrunk pore. However, the sintering time was impacted on the alumina distribution. This effect is illustrated in Figure 22.

**Figure 22** Size distribution by the different time sintering

As the Figure 22, the alumina distribution depended on the sintering time. The coarse pore size was developed in the membrane when time consuming was greater. The grains were growing when increasing sintering time thus the small particles were merged. However, 1 hour was sufficient sintering time what it was the small pore sized at the mono dispersion and coordinated in this study.

In order to prepare the favorite synthesize alumina, the appropriated state in the previous works were chosen. The repeated alumina was prepared by 1 mole Aluminum tri-sec butoxide in 12 mole i-butanol. Then, 0.3 mole ACAC was added drop wise into the mixed solution and 40 mole water was slowly adding to form gel networking at the final. The alumina characteristic is illustrated in Figure 23.

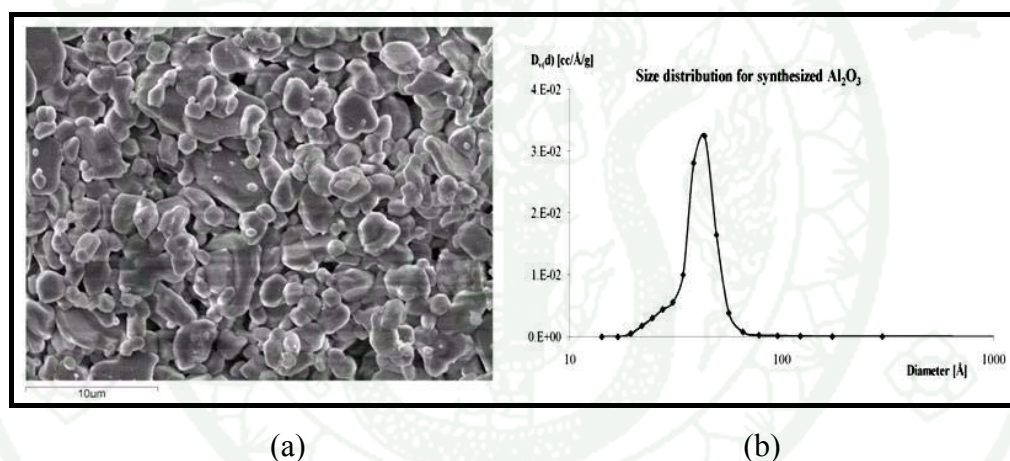


Figure 23 SEM photographs of synthesized alumina (a) and its size distribution (b)

In Figure 23, the synthesized aluminum alkoxide was kept for 2 day ageing to remove water and alcohol before sintering at 500 °C for 1 hour. The synthesized alumina was 36 Å alumina pore size, surface area 560.3 m²/g, pore volume 0.6 cc/g and mono dispersion.

2.4 Gas interaction performance

The gas performance was the comparative of gas adsorption through the alumina particles. The adsorption is the adhesion of molecules of gas, liquid, or

dissolved solids to a surface. This process accumulated the atoms on the surface of the adsorbent. However, atoms on the surface of the adsorbent were not wholly surrounded by other adsorbent atoms and therefore can attract adsorbents. The exact nature bonding depended on the species involved details. In this study, the adsorption of CO, CO₂, and H₂ was observed. The results are shown in Table 9.

Table 9 Gas adsorption (%) through the ceramic membrane layer

Item	CO	CO ₂	H ₂
Alumina disk	0.26	57.45	39.25
Synthesized alumina on disk	0.40	79.76	90.81

From the table 9, the adsorption was kept on synthesized greater than naked alumina disk. The alumina disk was inert which it prepared under the high approximately temperature about 1600°C while the synthesized alumina prepared at 500°C. The synthesized alumina was a high pore volume and enormous vacant area for gas collecting.

The synthesized alumina was prepared by sol-gel process that was usage as macroporous (pore size 20 - 500 Å) adsorbent. Thus, it was the gas adsorbent. The gas interaction was depended on the gas kinetic diameter. The H₂, CO₂ and CO were 28.9, 33.0, and 37.6 Å (Iwamoto, 2005), respectively. H₂ was the smallest kinetic diameter, the adsorption was 90.81%. CO₂ was the medium thus it was the moderate adsorption at 79.76%. CO was the biggest so the adsorption was very poor at 0.40%. In the elsewhere study, the researcher found that mesoporous (20-500 Å) alumina was a ceramic sorbent thus alumina membrane was adsorbed H₂ (Bai *et al.*, 1995) and well adsorbent for CO₂ (Iwamoto, 2005 and Faria *et al.*, 2008).

3. The integrated layer

There were three composite membrane layers in this work. The bottom was an alumina disk with 46% porosity. It used as supported layer. The second layer was a synthesized alumina, also. This layer was synthesized by sol-gel technique that it acted as a gas adsorption role. The topped layer was a catalytic membrane layer. It was formed by electrospinning process. It maintained as a catalyst in the water gas shift reaction. The magnification of each layer is displayed below.

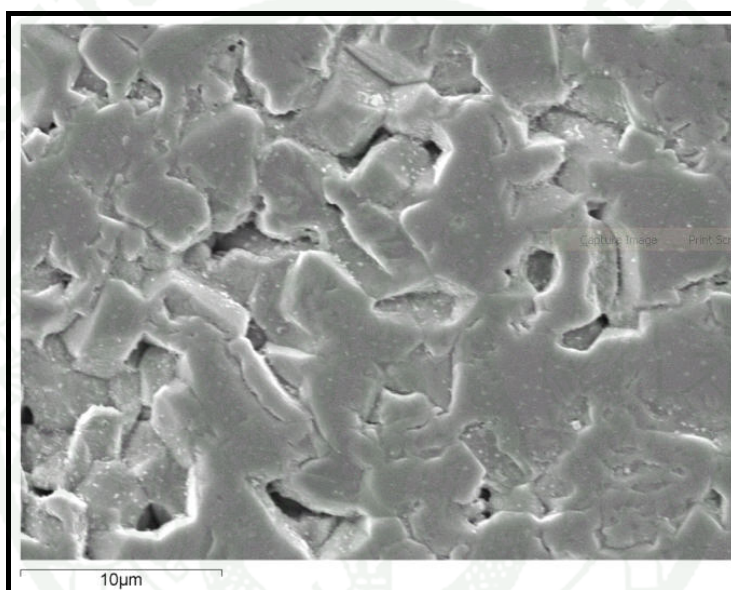


Figure 24 SEM photograph of alumina supported disk

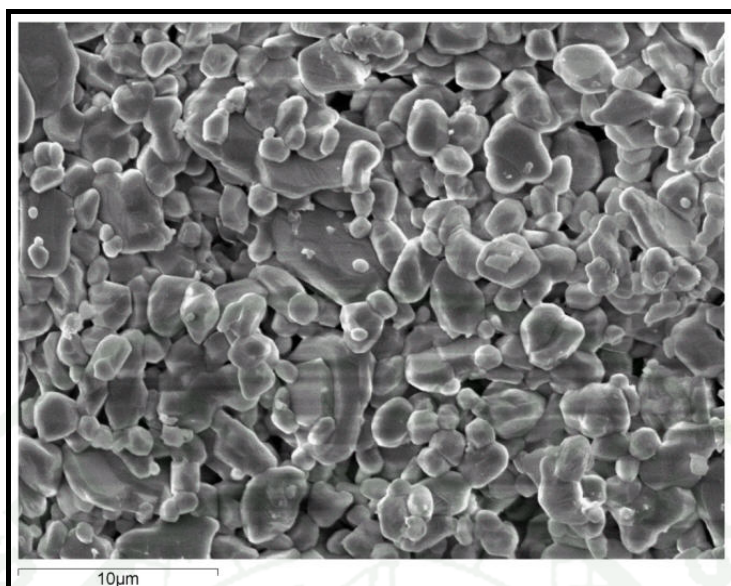
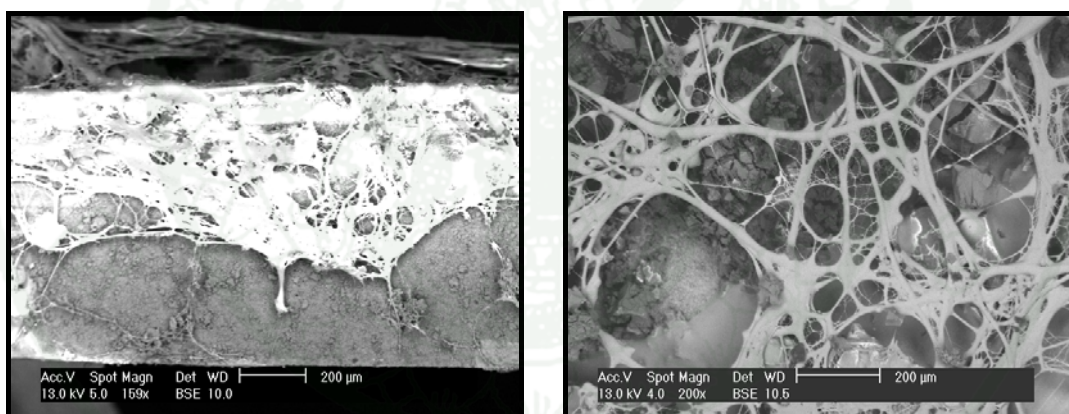


Figure 25 SEM photograph of synthesized alumina



(a)

(b)

Figure 26 SEM photographs of cross section (a) and topped view (b) of catalytic membrane layer

The alumina layer was composed integrated on the 1 mm thickness alumina supported disk by three times spin coating technique. The synthesized alumina was 1 mm thickness. The ceria electrospun fibers were coated onto an alumina layer with 0.3 mm thickness. Finally, HAuCl_4 was impregnated on the top membrane to

promote the reaction activity. The uniform catalytic membrane was applied in water gas shift reaction.

4. Water gas shift reaction performance

The performance in the water gas shift was verified. The fixed bed reactor, the catalytic reactor, and the hybrid membrane were compared. The overall catalyst (CeO_2) was 0.34 gram. The N_2 was flowing for 30 minutes at 250°C to reduce the catalyst prior the reaction running. The productivity reaction was reported by percentage of CO conversion (X_{CO}) at 250°C for 30 min., also. The gases occurring during the experiments were analyzed using Gas chromatography (GC), and the gas concentrations were calculated by the calibration curve determined in the appendix A.

The designed reactor was the firstly investigated on this experiment. The ceramic membrane reactor was spreading the catalyst on the synthesized alumina disk. The fixed bed reactor was a tubular tube which containing the pellet catalyst within. The catalyst was acting as the reactor shell. And, the hybrid membrane reactor was combining ceramic membrane reactor and fixed bed reactor together. The reactivity on ceramic membrane reactor was greater than the fixed bed membrane reactor. Nevertheless the adsorption was a lack of sympathy to distort the reaction performance on the ceramic membrane reactor but it was adsorbing the CO_2 in the water gas shift reaction cause of gas poisoning. However, the disk membranes have limited membrane areas (around 5 cm^2), leading to low conversions and yields. In order to increase the membrane area for oxygen storage, tubular reactors can be applied (Li *et al.*, 2008). The catalytic membrane layer was a significant problem in the reaction due to its physical property by coated on the layer. The coated catalytic was break down when contacted to stream for the time, that the reaction yield was rapidly dropping. The fixed bed was greater CO concentration but the CO_2 emitted more than the catalytic membrane reactor. According, the hybrid membrane was improvement reactor which combined the advantage of the both reactors. The

reaction was twice at the same reaction. The comparative on water gas shift reactor by the different reactors are presented in Figure 27.

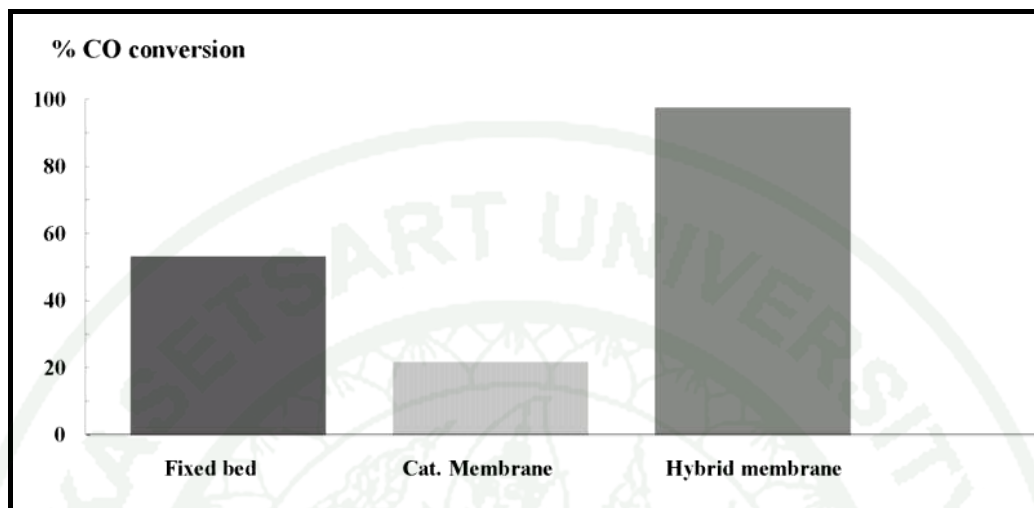


Figure 27 CO conversion (X_{CO}) by the different reactor type

In addition, Au/CeO₂ catalysts were the very active catalysts for the low temperature water gas shift reaction. These catalysts could be operated at even lower temperature than reduce the steady state CO content in thermodynamic equilibrium (El-Moemen *et al*, 2008). In the reduction of CeO₂ in catalysts, Ce⁴⁺ and oxygen vacancies most tend to provide electron being and improved the activation of molecules in the reaction. Addition, they could capture the H₂O and decompose it into -O and -OH which transferring to the active site on the surface and reacted with adsorbed CO to produce CO₂ and H₂O. It was known that the ceria was an oxygen storage role. The oxygen regeneration on ceria surface was a key step on the water gas shift reaction. The surface oxygen atom of ceria was essential to react with CO to produce CO₂.

Moreover, the temperature and time were a considerable parameter on the feed stream quality. Therefore, the associated factor was maintained by the reactor types. The examined temperatures were 225, 250, and 275°C. The times consideration were 15, 45, and 75 minutes, consequently. From the previous awareness, the low temperature water gas shift reaction was operated at 175 - 250°C.

Thus, the study found temperature among 225 and 250°C had a slightly differ reactivity. The CO conversion was the greatest yield at 250°C for the bulk reactors. The CO conversions are presented in Figure 28 – 31.

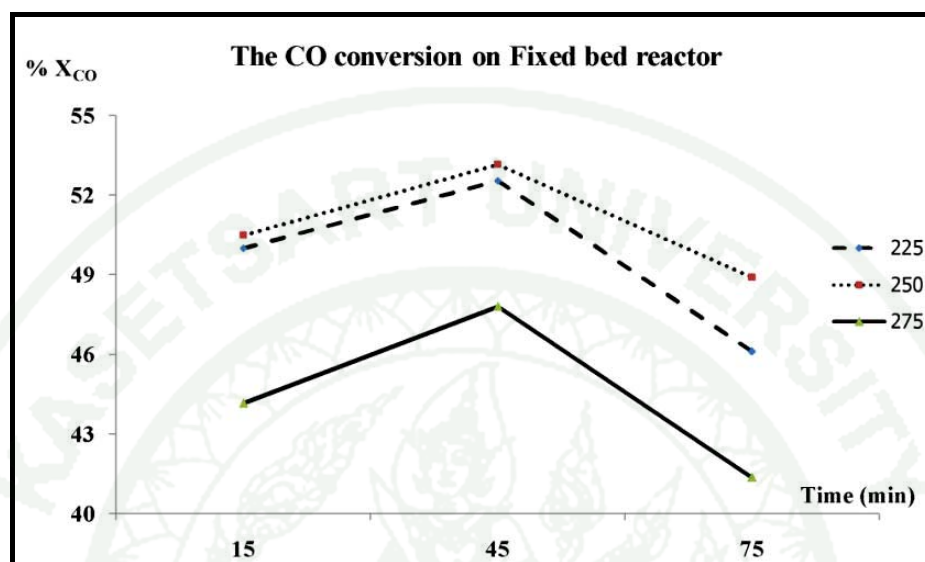


Figure 28 CO conversion (X_{CO}) on fixed bed reactor

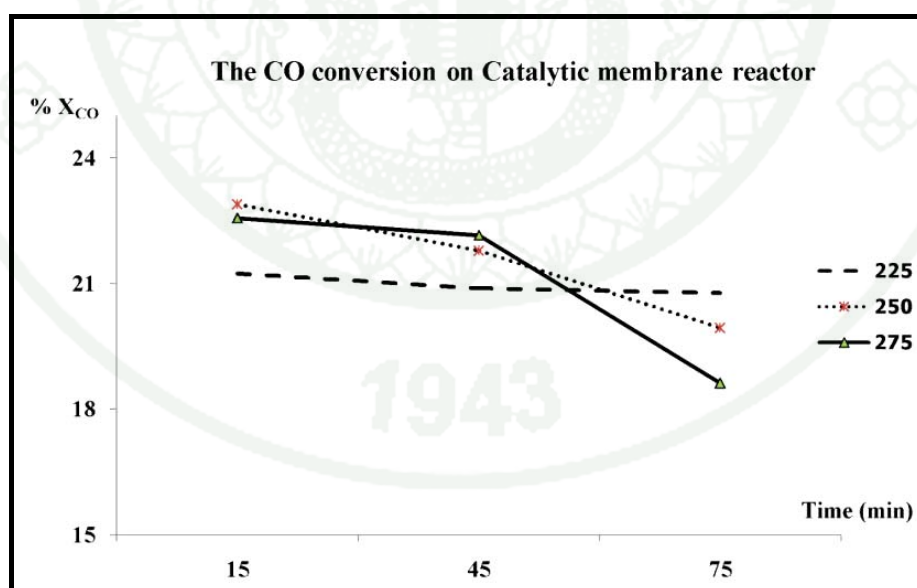


Figure 29 CO conversion (X_{CO}) on catalytic membrane reactor

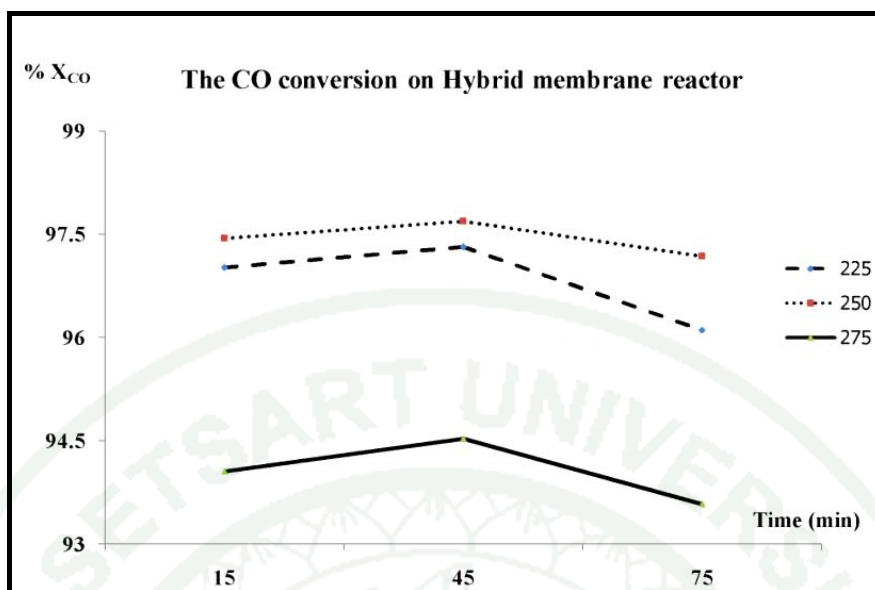


Figure 30 CO conversion (X_{CO}) on hybrid membrane reactor

The water gas shift reaction was two major reaction mechanisms. That was redox and formate mechanism. The formate reaction favored reacted at the high temperature, which barrier on the catalytic reaction. Hence, the catalysts deactivation was more dominant (El-Moemen *et al.*, 2008). In all case, the high temperature reduced activity of the Au/CeO₂ catalyst. Since, the reduction and re-oxidation of ceria was proposed to be dominant. The reduction in carbonate coverage the reaction inhibiting blocking of active site may be maintained.

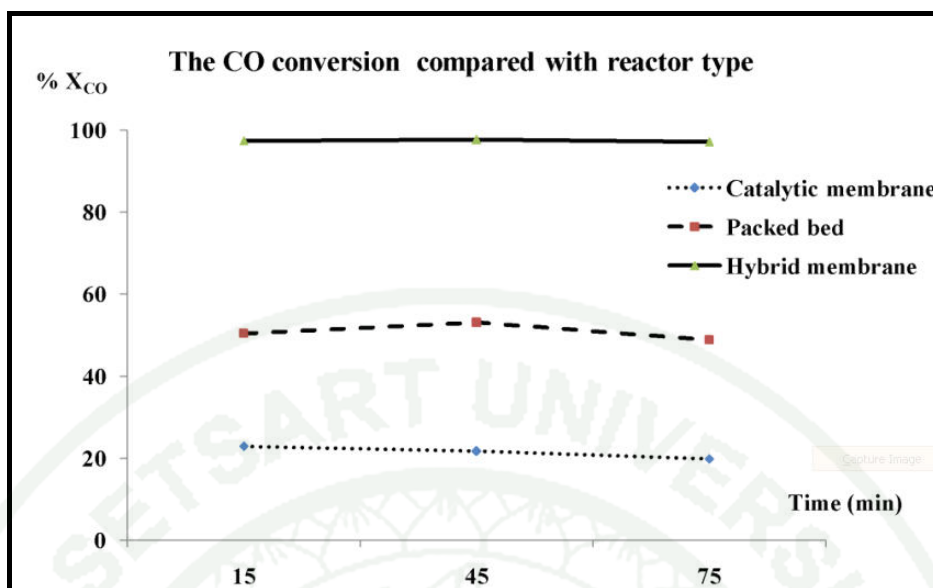


Figure 31 CO conversion (X_{CO}) at 250°C for 45 min

However, the type reactors were significant on CO conversion. The hybrid membrane reactor was the greatest CO conversion, when compared the CO conversion at 250°C. The time gave the high conversion was 45 minutes. The result is displayed in Figure 31. It showed that the increasing time was impacted on the carbonate forming in the water gas shift reaction, thus it reported earlier. The performance reactor could be arranged as hybrid reactor > fixed bed reactor > catalytic membrane reactor.

CONCLUSION AND RECOMMENDATIONS

Conclusion

From the experiment results and discussion indicated to achieve the research objectives. The finale outcome can be drawn into three parts as follows: 1) ceria electrospun fibers via electrospinning which the catalytic membrane layer 2) the synthesized alumina was prepared via sol-gel technique that act as mesoporous adsorption layer 3) the combination of electrospinning process and sol-gel technique were fabricated composite membrane layer for the water gas shift reaction. The particular section was displayed as following.

1. Ceria fibers synthesis and characterization via electrospinning

Electrospinning is a basic technique with the drawing of a polymer fluid, there are many different types of polymer and precursors that can be electrospun to form fibers. However, the other materials such as ceramic and carbon nanotubes required post processing of the electrospun fibers. The maintained properties depended on the type of raw materials.

Ceria (CeO_2) is a fluorite-structure oxide that can form extensive application. A simple and straightforward method providing high purity has been developed. CeO_2 fibers were successfully prepared by electrospinning technique. The solution property of the solvent had a prominent influence on the electrospinning process. The addition of the co-solvent thus i-propanol in water was reduced the surface tension of the feed solution and thereby promoted the polyvinyl alcohol (PVA) solubility. Smooth electrospun fibers were produced with 50 wt% i-propanol, 18 kV electricity consumed, and 8 centimeter distance between tip and aluminum ground collector. The CeO_2 fibers were obtained by calcined at 450°C for 3 hours. They had an average diameter around 600 ± 80 nm. The EDS and XRD results were verified the formation of CeO_2 .

As each of the properties involved in electrospinning is a vast science of its own. The high surface area per unit volume is majority material goods using as catalytic material.

2. Alumina ceramic supporter fabrication via sol-gel technique

Sol-gel technique is an attractive alternative to other methods for synthesis of ceramics and glasses. It is very useful for thin film deposition because of the capability to coat materials of various shapes. The process started with processing of dense, bulk materials, and great efforts have been made on how to density porous gels into glasses and ceramics. However, recently sol-gel processing of mesoporous and macroporous materials has also attracted much attention, including materials with well-controlled pore characteristics and highly porous materials, which have excellent chemical and photonic functions.

The synthesized alumina was prepared by 1 mol aluminum tri-sec butoxide, 0.3 mol ACAC, 40 mol water, 2 days ageing at the room temperature, and sintering at 500°C for 1 hour. It had the pore size diameter as 36 Å, surface area 560.3 m²/g, pore volume 0.6 cc/g and mono dispersion. The alumina characteristics were using N₂ adsorption-desorption isotherms by an Autosorb-1C. The synthesized was coated onto alumina supported disk by spin coating technique. Thus, it could adsorb CO₂ and H₂ well done at 250°C for 30 min. The composite alumina disk was repeated coat by CeO₂ electrospun fibers and impregnated with HAuCl₄ to promote the ceramic membrane layer. The ceramic membrane layer was an essential component for the water gas shift reaction.

3. The catalytic performance on water gas shift reaction

The performance on water gas shift reactor was verified into two factors. These were the reactor types and the operating condition on the water gas shift reaction. The reactor types were indicated the arrangement and catalytic packing. The catalyst pellets were packed into the stainless steel tubular reactor for fixed bed membrane reactor. The reaction was moderate CO conversion but the CO₂ occurring

was mixed and detected at the outlet stream. Thus, the CO₂ was a hazard gas cause blocking the oxygen transportation when human breathing. The electrospun fibers catalyst was spread onto the alumina disk for catalytic membrane reactor. That was high active area for reaction activity but the CO₂ was adsorbed on the synthesis alumina. Thus the CO conversion was slightly. The catalytic membrane reactor had two functions consist during reaction occurring. These were reaction at the catalytic membrane layer and adsorption at the synthesized alumina membrane layer. The hybrid membrane reactor was an improvement reactor. They combined the advantages of fixed bed membrane reactor and ceramic membrane reactor simultaneous. The design was the first run as fixed bed membrane reactor then it was connected to the ceramic membrane reactor. There was double reaction in the hybrid membrane reactor that favored reaction performance.

Addition, the reaction performances were compared by temperature and time working at the different reactor types. All of the reactors seemed the similar trends. They were well done at 250°C for 45 minutes and the reaction decreased at the higher temperature. The results were explained by Au deactivate and carbonate coverage the reaction thus it was inhibit blocking of catalyst active site. However, at 225°C the reaction performance was not remarkable what it was the nearly water gas shift reaction favorite from the previous reported. Therefore, the reaction performance was presented the hybrid membrane reactor > fixed bed membrane reactor > catalytic membrane reactor. The CO conversions were 97.69, 52.31, and 21.78, respectively.

Recommendations

Even though the results indicate a new finding fabrication materials for water gas shift reaction. The extended worked and released the difficulty item of the study would be declared as follow:

1. The electrospun fibers would be the different uniform depended on the operating condition. The interconnected electrospun fiber was fabricated by the low distance or the low electrical supply what it was interested in scaffold application. Addition, the needless electrospinning technique was an alternative selection to

establish the mass production for electrospun fibers. However, the electrospinning process was dangerous hence the operator would be careful during the process.

2. The sol-gel technique with aluminum tri-sec-butoxide was a rapid reaction performed. The process was operated under N_2 to avoid the reaction with oxygen. The parameters e.g. the precursor type and concentration, time, and temperature at the both ageing condition and sintering process were carried out to gel network formation. The other, the mixed another precursor such as activated carbon would be improvement the adsorption properties and varied application.

3. The measured performance on the reaction should be using online gas chromatography to avoid the disturb noise. And, the further could be compared the other precious metals e.g. Pt, Ag on CeO_2 or the co-catalyst of Au on the other metal oxide e.g. Al_2O_3 .

LITERATURE CITED

- Acatay, K., S. Eren, A. Mert and Z. Yusuf. 2003. **Electrospinning of low surface energy quaternary ammonium salt containing polymers and their antibacterial activity**. Proceedings of the NATO Advanced Study Institute, Belek-Antalya, Turkey. Nato Science Series II, Mathematics, Physics and Chemistry 169: 97-106.
- Aguila, G., S. Guerrero and P. Araya. 2008. Influence of the crystalline structure of ZrO_2 on the activity of Cu/ZrO_2 catalysts on the water gas shift reaction. **Catalytic communication**. 9: 2550-2554.
- Ahmad, A.L., N.F. Idrus and M.R. Othman. 2005. Preparation of perovskite alumina ceramic membrane using sol-gel method. **Membrane science**. 262: 129-137.
- Araujo, F.G., G.P., LaTorre and L.L., Hench. 1994. Structural evolution of a porous type-VI sol-gel silica glass. **Journal of Non-Crystalline Solids**. 185: 41-48.
- Andrea, M., D. Farias, P. Bargiela, M. Rocha and M. Fraga. 2008. Vanadium-promoted Pt/CeO_2 catalyst for water-gas shift reaction. *In press* **Journal of Catalysis**.
- Bae, B.S. 2008. **Sol-gel nano materials and process., In MS512 Nanotechnology**. Korea.
- Basile, A., A. Criscuoli, F. Santella and E. Drioli. 1996. Membrane reactor for water gas shift reaction. **Gas separation Purification**. 4: 243-254.
- Bai, C., M.D., Jia, J.L., Falconer and R.D., Noble. 1995. Preparation and separation properties of silicalite composite membranes. **Journal of Membrane Science**. 105: 79-87.

- Bickford, E.S., V. Subramani and S. Chunshan. 2005. Nano-structured CeO₂ supported Cu-Pd bimetallic catalysts for the oxygen-assisted water-gas-shift reaction. **Catalysis Today**. 99: 347-357.
- Bunluesin, T., R.J. Gorte and G.W. Graham. 1998. Studies of the water-gas-shift reaction on ceria-supported Pt, Pd, and Rh: implications for oxygen-storage properties. **Applied catalysis B: Environmental**. 15: 107-114.
- Callaghan, C.A. 2006. **Kinetics and Catalysis of the Water-Gas-Shift Reaction: A Microkinetic and Graph Theoretic Approach**. Worcester Polytechnic Institute. England.
- Chen, Y., J. Cheng., P. Hu. and H. Wang. 2008. Examining the redox and formate mechanisms for water-gas shift reaction on Au/CeO₂ using density function theory. **Surface Science**. 602: 2828-2834.
- Clipper Controls Inc. 2005. **Dielectric Constant Reference Guide**. San Francisco, USA.
- Dharmaraj, N., H.C. Park, C.K. Kim, H.Y. Kim and D.R. Lee. 2004. Nickel tatanate nanofibers by electrospinning. **Materials chemistry and physics**. 87: 5-7.
- Ding, B., K.K. Chul, Y.K. Hak, K.S. Ming and J.P. Soo. 2004. Titanium dioxide nanofibers prepared by using electrospinning method. **Fibers and polymers**. 2 (5): 105-109.
- El-Moemen, A., A. Karpenko, Y. Denkwitz and R.J. Behm. 2008. Activity, stability and deactivation behavior of Au/CeO₂ catalysts in the water gas shift reaction at increased reaction temperature (300°C), *In press*, **Journal of Power Source**.
- Faria, C.L.L., T.K.R., Oliveira, V.L., Santos and C.A., Rosa. 2008. Usage of the sol-gel process on the fabrication of macroporous adsorbent activated-gamma alumina spheres. *In press*, **Microporous and Mesoporous Materials**.

- Frusteri, F., C. Espro, F. Arena, E. Passlacqua, A. Patti and A. Parmaliana. 2000. Partial oxidation of propane on nafion supported catalytic membranes. **Catalysis today**. 61: 37-41.
- Grafe, G. H.G. Timothy and M.G. Kriistine. 2003. Nonwovens in filtration. *In* **Association of Nonwovens and Engineered Fabrics Fifth International Conference**. Germany.
- Gonzalez, I.D., R.M. Navarro, M.C. Alvarez-Galvan, F. Rosa and J.L.G. Fierro. 2008. Performance enhancement in the water-gas shift reaction of platinum deposited over a cerium-modified TiO₂ support. **Catalysis Communications**. 9: 1759-1765.
- Heterogeneous Catalysis Research group. 2004. **Fuel cell and catalysis**. Ohio state university.
- Hung, C.M. 2008. Catalytic Decomposition of Ammonia over Bimetallic CuO/CeO₂ Nanoparticle Catalyst. **Aerosol and Air Quality Research**. 8: 447-458
- Iwamoto, Y. 2005. **Inorganic Membranes for CO₂ and H₂ Separation**. *In* RITE International Seminar, Japan. January 14, 2005.
- Jacobs, G., U. Graham, and B.H. Davis. 2002. **In-situ DRIFTS investigation of Pt/CeO₂ catalysts for low temperature WGS**. *In* Tri-State Catalyst Social Spring Symposium. USA.
- Karnik, Sooraj V., Miltiadis K. Hatalis and Mayuresh V. Kothare. 2001. Palladium based micro-membrane for water gas shift reaction and hydrogen gas separation, pp. 1-8. *In* **international conference on microreaction technology 5 ed**. Strasbourg, France.
- Kikuchi, E. and S. Ueimeya. 1991. Double tubular type membrane reactor. **J.membrane**. 56: 303-313.

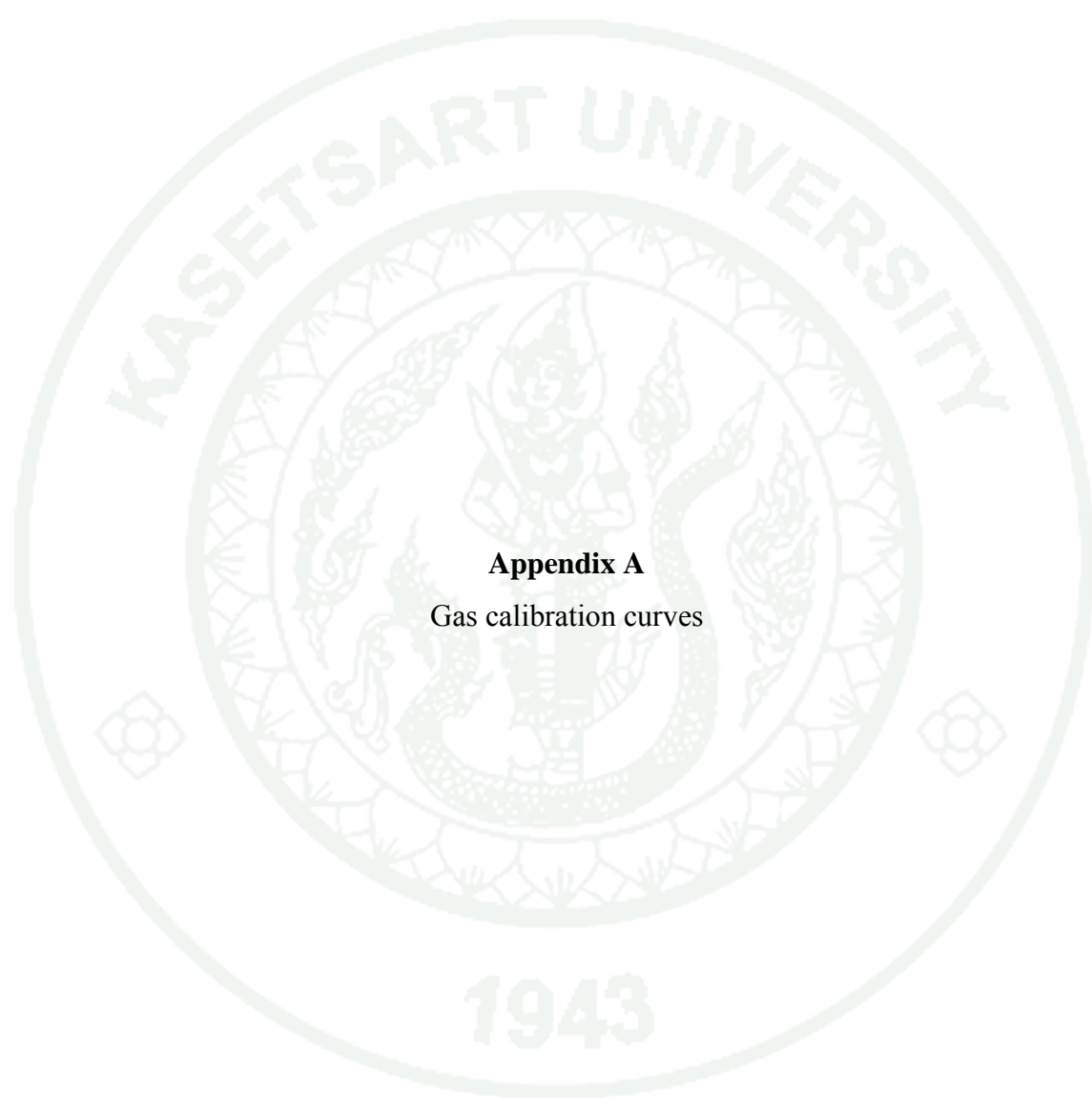
- Klein, L.C. 1991. Sol-Gel Coatings, *In* Satas, D. **Coating Technology Handbook**. Marcel Dekker, Inc., USA.
- Li, J., Y. Zhan, X. Lin and Q. Zheng. 2008. Influence of calcinations temperature on properties of Au/Fe₂O₃ catalysts for low temperature water gas shift reaction. **Acta Physico-Chemica Sinica**. 24: 932-938.
- Li, K. 2007. **Ceramic membrane for separation and reaction**. John Wiley & Sons, Ltd., England.
- Lilong J., Y.E. Binghuo and W. Kamie. 2008. Effects of CeO₂ on structure and properties of Ni-Mn-K/bauxite catalysts for water-gas shift reaction. **Journal of rare earth**. 26: 352-356.
- Mazaheri M., A.M. Zahedi, M. Haghighatzadeh and S.K. Sadrenzhaad. 2008. Sintering of titania nanoceramic: Densification and grain growth. **Ceramic international**. 35: 685-691.
- Michael, G.B., H.S. Caram and S. Sircar. 2009. Selection of CO₂ chemisorbent for fuel-cell grade H₂ production by sorption-enhanced water gas shift reaction. **journal of hydrogen energy**. 34: 2972–2978
- Milovzorov, D.V. 2008. Field effect on crystal phase of silicon in Si/CeO₂/SiO₂ structure. **Journal of Nanomaterials**. 19: 435-442.
- Park, J.N., J.H., Kim and H.I., Lee. 2000. A study on the Sulfur-Resistant Catalysts for Water Gas Shift Reaction III. Modification of Mo/ γ -Al₂O₃ Catalyst with Iron Group Metals. **Bull. Korean Chem. Soc**. 21: 1233-1238.
- Peterlik, H., H. Rennhofer, V. Torma and U. Bauer, 2007. Structural investigation of alumina silica mixed oxide gels prepared from organically modified precursors. *Journal of Non-crystalline Solids*. 353: 1635-1644.

- Pina, M., M. Menendez and J. Santamaria. 1996. The Knudsen-diffusion catalytic membrane reactor: an efficient contactor for the combustion of volatile organic compounds. **Applied catalyst B**. 11: 19-27.
- Ramakrishna S., K. Fujihara, W.E. Teo, T.C. Lim and Z. Ma. 2005. **An introduction to electrospinning and nanofibers**. World scientific publishing Co.Pte.Ltd, Singapore. 90-116.
- Radhakrishnan, R., R.R. Willigan, Z. Dardas and T.H. Vanderspurt. 2006. Water gas shift activity and kinetics of Pt/Re catalysts supported on ceria-zirconia oxides. **Applied Catalysis B:Environmental**. 66: 23-28.
- Reddy, B.M. and A. Khan. 2005. Nanosized CeO₂-SiO₂, CeO₂-TiO₂, and CeO₂-ZrO₂ Mixed Oxides: Influence of Supporting Oxide on Thermal Stability and Oxygen Storage Properties of Ceria. **Catalysis Surveys from Asia**. 9: 155-171.
- Ruhi, G., O.P., Modi, A.S.K., Sinha and I.B.,Singh. 2007. Effect of sintering temperatures on corrosion and wear properties of sol-gel alumina coatings on surface pre-treated mild steel. *In press*, **Corrosion Science**.
- Saracco, G. and V. Specchia. 1995. Catalytic ceramic filters for flue gas cleaning, **Catalytic performance and modeling of Industrial Engineering Chemistry**. 34:1480-1487.
- Shao, C., G. Hongyu, L. Yichun, G. Jian, Y. Na and Y. Xinghua. 2004. A novel method for making ZrO₂ nanofibers via an electrospinning technique. **Crystal growth**. 267: 380-384.
- Splinter, A., J. Sturmman, O. Bartels and W. Benecke. 2002. Micro membrane reactor: a flow-through membrane for gas pre-combustion. **Sens. Actuators, B**. 83:169-174.
- Thompson group, 2006. **Carbide and nitride supported catalysts for water-gas-shift**. Michigan university, USA.

- Tsuru T., T. Kan-no, T. Yoshioka and M. Asaeda. 2003. A photocatalytic membrane reactor for gas-phase reactions using porous titanium oxide membranes, **Catalyst today**. 82: 41-48.
- Theodore, L. and R.G. Kunz. 2005. **Nanotechnology: Environmental Implications and Solutions**. John Wiley&Sons, Inc., New Jersey.
- Wittayakhun, J. and K. Nurak. 2004. **Catalysis: Fundamentals and Applications**Thammasat University printed. Bangkok, Thailand.
- Wen, Q.Y., H.W., Zhang, Q.H., Yang, S., Li, D.G., Xu and J.Q., Yao. 2009. Fe-Doped Polycrystalline CeO₂ as Terahertz Optical Material. **Chinese Phys. Letter**. 26: 803-806.
- Yang, Q.B., D.M. Li, Y.L. Hong, C. Wang, S.L. Qui and Y. Wei. 2003. Preparation and characterization of a PAN nanofiber containing Ag nanoparticles via electrospinning. **Synthetic metals**. 137: 973-974.
- Yamada M., K. Fugii, H. Haru and K. Itabashi. 1988. Preparation and catalytic properties of special alumina membrane formed by anodic oxidation of aluminum. **Chemical Engineering and Processing: Process Intensification**.
- Yuan, Z.Y., V. Idakiev, A. Vantomme, T. Tabakova, T.Z. Ren and B.L. Su. 2007. Mesoporous and nanostructures CeO₂ as supports of nano-sized gold catalysts for low-temperature water gas-shift reaction. **Catalysis Today**. 131: 203-210.
- Zalamea S., M. Pina, A. Villellas, M. Menndez and J. Santamara. 1999. Combustion of volatile organic compounds over mixed-regime catalytic membranes. **Reaction kinetic catalyst letter**. 67: 13-19.
- Zhao, D., E. Han, X. Wu and H. Guan. 2006. Hydrothermal synthesis of ceria nano- particles supported on carbon nanotubes in supercritical water. **Materials Letters**. 60: 3544–3547.



APPENDICES



Appendix A

Gas calibration curves

Gas calibration curves

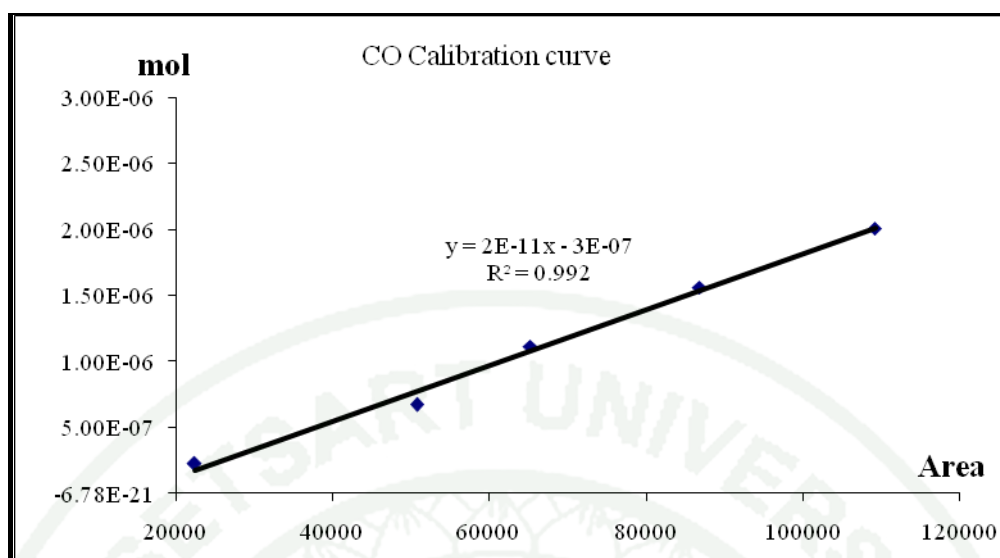
Sample gas were prepared and collected in a gas sample. For CO, CO₂, H₂, gas, the most volume of the sample gas prepared were 0.2, 0.4, 0.6, 0.8, and 1.0 ml. However, the concentration of H₂ was not detected at the under low volume preparing. The H₂ volume would be 0.4, 0.5, 0.6, 0.8, and 1.0 ml. The concentration of sample gases was measured using a gas chromatography (GC). The results obtained were used to establish the calibration curve for each gas.

1. Calibration curve of CO gas

The CO gas was 5% concentration in the whole gas was chosen as a standard gas in this section.

Appendix Table A1 CO calibration curve

Volume (ml)	Area	CO (mol)
0.1	22,394	2.23E-07
0.3	50,759	6.70E-07
0.5	65,225	1.12E-06
0.7	86,781	1.56E-06
0.9	109,147	2.01E-06



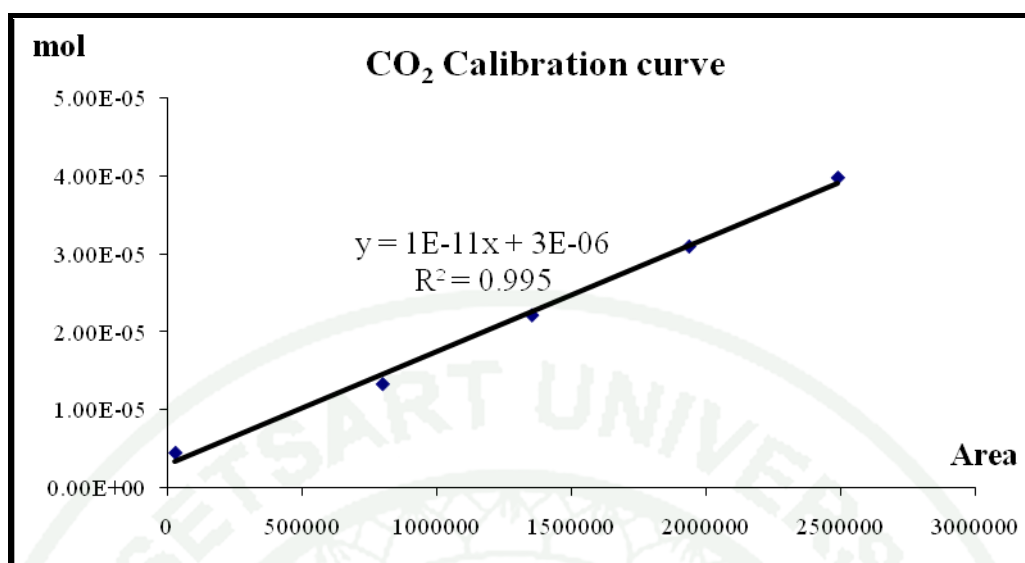
Appendix Figure A1 CO Calibration curve

2. Calibration curve of CO₂ gas

The CO₂ gas was 99% concentration in the whole gas was chosen as a standard gas in this section.

Appendix Table A2 CO₂ calibration curve

Volume (ml)	Area	CO ₂ (mol)
0.1	28,050	4.42E-06
0.3	797,117	1.33E-05
0.5	1,351,184	2.21E-05
0.7	1,934,334	3.09E-05
0.9	2,486,373	3.98E-05



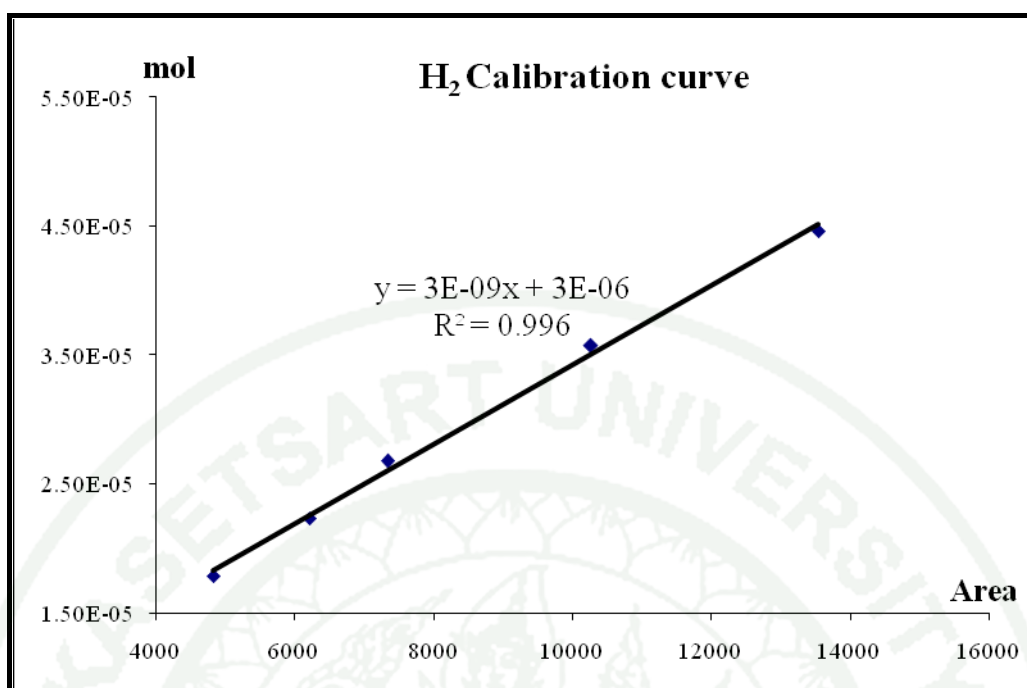
Appendix Figure 2 CO₂ Calibration curve

3. Calibration curve of H₂ gas

The H₂ gas was 99.99% concentration in the whole gas was chosen as a standard gas in this section.

Appendix Table A3 H₂ calibration curve

Volume (ml)	Area	H ₂ (mol)
0.4	4,823	1.79E-05
0.5	6,213	2.23E-05
0.6	7,341	2.68E-05
0.8	10,267	3.57E-05
1.0	13,545	4.46E-05



Appendix Figure A3 H₂ Calibration curve



Appendix B

Water gas shift reaction process

The water gas shift reaction process

Table Appendix B1. The reactor comparative on the water gas shift reaction

Reactor Type	CO (μmol)	CO (ppm)	CO ₂ (μmol)	H ₂ (μmol)	%CO Conversion
Blank	8.22	46.03	3.03	0.00	0.00
Packed Bed	3.85	21.95	6.10	20.20	53.16
Membrane	6.43	36.01	2.06	7.95	21.78
Hybrid	0.19	1.06	3.02	23.76	97.69

Table Appendix B2. The water gas shift condition

Reactor type	Temp (°C)	X _{co} (%)		
		15 min	45 min	75 min
Catalytic membrane	225	21.24	20.89	20.78
	250	22.89	21.78	19.94
	275	22.56	22.15	18.62
Packed bed	225	50.00	52.55	46.11
	250	50.49	53.16	48.91
	275	44.16	47.81	41.36
Hybrid membrane	225	97.02	97.32	96.11
	250	97.44	97.69	97.18
	275	94.06	94.53	93.58

CURRICULUM VITAE

NAME : Ms. Kanchana Luepong

BIRTH DATE : December 10, 1974

BIRTH PLACE : Bangkok, Thailand

EDUCATION	: <u>YEAR</u>	<u>INSTITUTE</u>	<u>DEGREE/DIPLOMA</u>
	1994	Rajamangala Institute of technology	B.Eng. (Textile chemistry Engineering)
	1999	Chulalongkorn University	M.Eng. (Chemical Engineering)
	2010	Kasetsart University	D.Eng. (Chemical Engineering)

POSITION/TITLE : Lecturer

WORK PLACE : Faculty of Industrial Textiles and Fashion Design,
Rajamangala University of Technology Phra
Nakhon.